Evaluating and constraining the effects of Paleozoic crustal scale structural features on the fault kinematics and basin evolution of the Dutch Central Graben.

A MSc. Thesis by David Borghouts

July 13, 2019
Department of Geosciences, Utrecht University

Supervised by:
Jeroen Smit, Department of Geosciences, Utrecht University
Prof. Dimitrios Sokoutis, Department of Geosciences, Utrecht University

Table of contents

1. Abstract

This study aimed to achieve a better understanding on how reactivated Paleozoic structure in the subsurface of the southern North Sea influenced the placement and the evolution of the Dutch Central Graben basin. The Dutch Central Graben basin opened during the Permian-Triassic transition as part of the larger North Sea rift system and is situated above the suture between the coalesced terranes of Baltica and Avalonia. By using analogue tectonic modelling, the results of this study show that fault distribution within the Dutch Central Graben basin suggest that the basin formed along a preexisting detachment of Paleozoic age. Furthermore, results show the interplay between this detachment and the interface between the ductile lower crust and brittle upper crust Avalonia, determined the placement and opening of the Dutch Central Graben. Finally, the results of this study suggest that although it is difficult to recreate using analogue modelling, that this preexisting Paleozoic detachment is likely to be a reactivated thrust structure that formed as part of a Caledonian orogenic complex that marks the transition between Avalonia and Baltica.
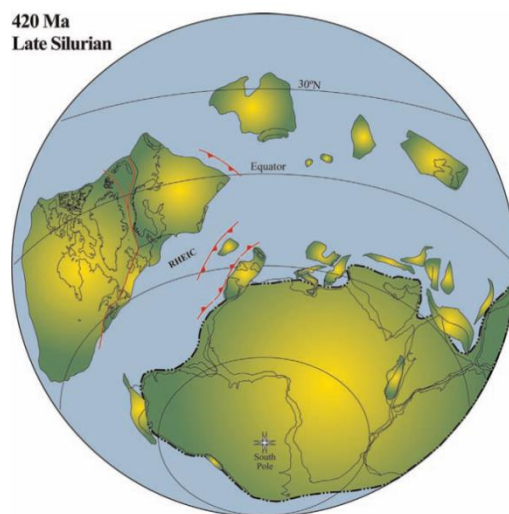
2. Introduction

The North Sea is characterized by the presence of a number of deep rift basins, that initiated during the Permian-Triassic transition as part of the Mesozoic North Sea rift, a failed arm of the Atlantic-North Atlantic rift system (Ziegler, 1992). One of these basins, the Dutch Central Graben (DCG), located in the southern North Sea has been historically defined as a symmetrical Mesozoic rift basin, based on the Mesozoic sedimentary infill geometry (Ziegler and Kent, 1982). Also, a lack of proper reflection seismic data due to the presence of a thick succession of Permian evaporates resulted in a poor understanding of deeper Paleozoic crustal features below the Dutch Central Graben. Since then, advancements in deep crustal interpretations from reflection and refraction profiles have allowed for a better constraint on these Paleozoic crustal structures (eg., Mona Lisa Working Group, 1997a, 1997b). These show that the Dutch Central Graben is in fact asymmetric in nature and is bounded on its eastern flank by a SW dipping detachment that reaches MOHO depth, known as the Coffee Soil Fault (CSF). Recent results from potential field modelling and seismic velocities studies (Lyngsie and Thybo, 2007; Smit et al., 2016) suggest that this detachment is coincident with the Caledonian Thor suture, which is the result of the microplate Avalonia being thrust over Baltica in a ramp-flat-ramp geometry. This would mean that the opening and location of the Dutch Central Graben was accommodated or at least partially influenced by the reactivation of Paleozoic structures situated in deeper crustal settings (eg., Van Wijhe, 1987; Lyngsie et al., 2006; van Winden et al., 2018). The exact relation between these Paleozoic structures and the kinematics of basin opening and development is not fully understood. Therefore this study is particularly interested in providing better insight in the link between these Paleozoic structures on the evolution of the well documented Mesozoic Dutch Central Graben basin by solving the following issues in three series of experiments using analogue tectonic modelling:

(1) Evaluating how the overall geometry of these Paleozoic structures determines the temporal and structural distribution and evolution of faulting in the Dutch Central Graben by using analogue tectonic modelling in an extensional setting over a predetermined detachment, using the documented geometry of the Paleozoic structures (2) How on a crustal scale these Paleozoic structures determined basin opening and the location of the Dutch Central Graben, by using analogue modelling on a crustal scale. (3) Whether it is possible to model the reactivation of thrust faults in an analogue model and if so, what this can tell us about the formation of these Paleozoic structures.

3.1 Paleozoic

The crust beneath the Dutch Central Graben is comprised of an assembly of the paleocontinents Laurentia, Baltica and Avalonia. These terranes coalesced during the Caledonian orogeny in the Late Ordovician to Early Devonian to form the Laurussian or Euramerican continent (Ziegler, 1990b). Prior to the Caledonian orogenic phase the microcontinents Baltica and Avalonia were separated by the Tornquist Ocean. The Tornquist ocean started to narrow during Ordovician times and fully closed by oblique soft docking of Avalonia to Baltica around the Ordovician-Silurian boundary (Torsvik et al., 1996). The now combined Baltica-Avalonia started to merge with Laurentia during the Silurian when the Iapetus ocean that separated these two continents closed to finally form the Laurussian continent. During Devonian time up to early Carboniferous times the Laurussian continent was separated from Gondwana by the Rheic Ocean. The onset of the closure of the Rheic ocean started in the late Devonian and culminated during the late Carboniferous Variscan orogeny when Laurussia collided with Gondwana to form the Pangea supercontinent (Ziegler, 1990b; Cocks and Torsvik, 2007). During the late Permian the North Sea area experienced an episode of significant subsidence due to cooling of the lithosphere. This created an east-west trending basin that stretched from modern day Britain to Poland (Ziegler, 1990a; Geluk, 2005) known as the Southern Permian Basin (SPB). Towards the end of the Permian the SPB had moved North to a latitude of 20° where it experienced predominantly arid conditions(Wong et al., 2007). During this time of the Pangea supercontinent, the SPB was surrounded by landmasses, effectively isolating it from surrounding waters. The SPB would periodically receive an influx of water from surrounding seas that led to the deposition of a thick succession of evaporates known as the Zechstein Group that ranges in thickness from 50m in southern Netherlands, to over 1200m in the Northern Dutch offshore (Geluk, 2005).

Figure 1 Paleogeographic map of the Late Silurian showing the coalesced terranes of Baltica-Avalonia and Laurentia in the Laurussian continent. During this time the Laurussian continent was separated from Gondwana by the Rheic ocean figure from Cocks et al., 2007

3.2 Mesozoic

The Early Triassic breakup of the Pangean supercontinent ensued large regional stresses across western and central Europe. As a result, a branch of the Norwegian-Greenland Sea rift propagated into the North Sea area, which led to an E-W rifting phase during the Middle and Late Triassic (Ziegler, 1990a, 1992). During this time several basins in the North Sea area opened, one of them being the Dutch Central Graben (DCG). This initial phase of extension was followed by a period of relative tectonic quiescence during which regional thermal subsidence prevailed and sedimentary infill of the basins in the North Sea area gradually continued with occasional interruption of active faulting (Geluk, 2005). Doming during the Middle Jurassic led to regional uplift and subsequent erosion, creating the Mid-Kimmerian unconformity. Only local depocenters such as the DCG received an influx of sediments during this time, which explains why the DCG has a complete Jurassic succession (Ziegler, 1992; van Winden et al., 2018). Rifting in the North Sea area peaked during the Late Jurassic-Early Cretaceous characterized by the formation of NW-SE trending faults. This rifting waned during the later stages of the Cretaceous when the extensional stresses were concentrated in the Atlantic domain (Ziegler, 1990b).
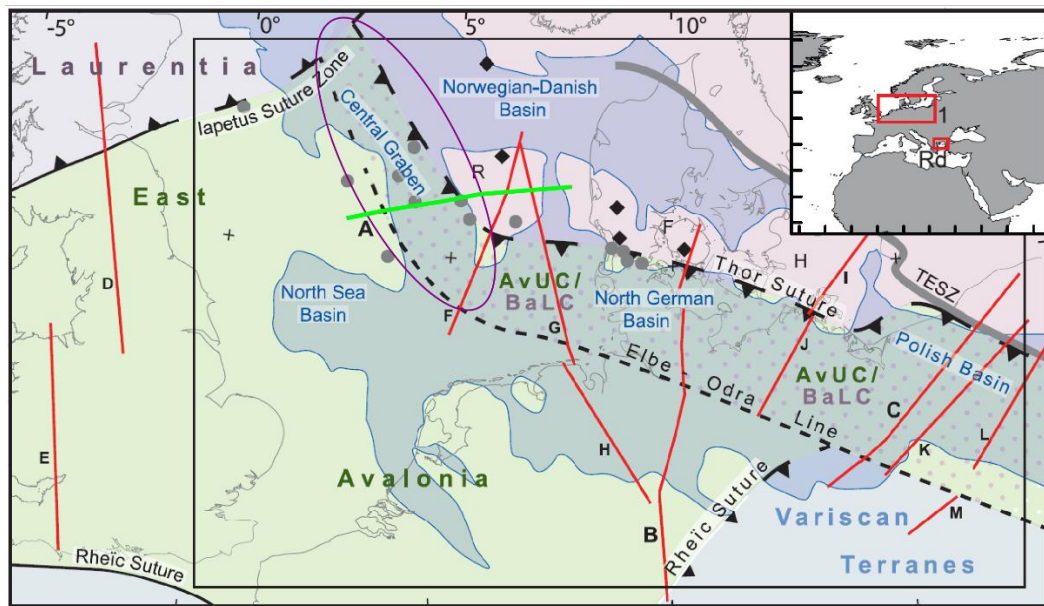

Figure 2 Map view of the location of the Dutch Central Graben marked by the purple ellipse. Green line marks the transect of the MONA LISA-3 profile.

3.3 Thor Suture Zone

The Thor suture zone (TSZ), the north-western branch of the Trans-European suture zone, marks the closure of the Tornquist ocean during Ordovician-Silurian times and separates the paleocontinents of Baltica and Avolonia (Berthelsen, 1998; Williamson et al., 2002; Smit et al., 2016). The TSZ was formed by the southward subduction of Baltica under Avalonia (Smit et al., 2016). The TSZ is covered by deep basins filled with Late Paleozoic-Holocene sediments making its exact location and geometry difficult to interpret(Torsvik and Rehnström, 2003; Lyngsie and Thybo, 2007; Smit et al., 2016). Deep seismics indicate the presence of a SW dipping crustal reflector that is likely to correspond to the TSZ (Mona Lisa Working Group, 1997a, 1997b). A combination of gravity and magnetic modelling indicates the presence of a sharp curved planar interface that reaches to MOHO depth with an average dip of 14° (Williamson et al., 2002). By applying a reconstruction to the interpreted MONA LISA-3 profile an average angle of 12° can be obtained (*fig. 3*).
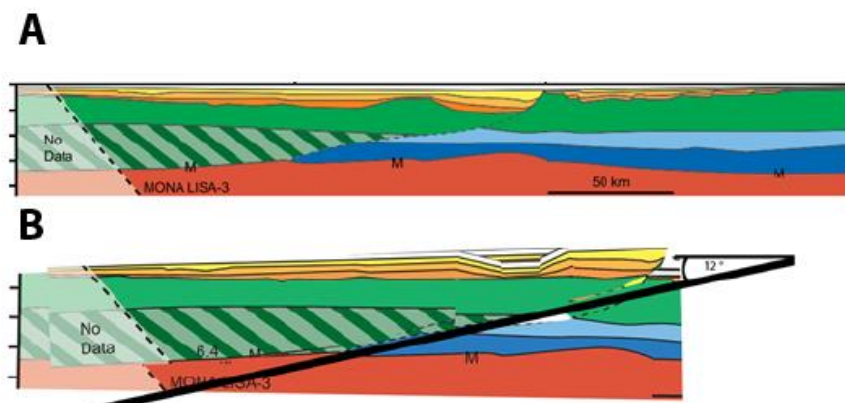

Figure 3 A) Interpreted MONA LISA-3 profile of present day situation obtained from (Smit et al., 2016) **B) Reconstruction of ML-3 Profile showing average ramp angle of 12°.**

4. Methods

4.1 Analogue modelling

Analogue tectonic modelling was used to study the effects of preexisting structural features on the distribution, geometry and temporal evolution of faulting in the extensional basin setting of the Dutch Central Graben. A separate set of experiments was designed to test whether thrust faults can be reactivated as low angle normal faults on a crustal scale. Finally, a set of experiments was executed to study the influence of preexisting structures on the location of basin initiation of the Dutch Central Graben.

4.2 Experimental set-up

The experiments were constructed on a fixed horizontal table. Deformation was applied by pulling a plastic sheet from under the models at constant velocity. The models where all 30 cm wide with metal bars bounding the sides. Models were made of horizontal sand layers, to some experiments a basal silicone putty layer was added to model ductile behavior of salt layers or lower crust. A camera was positioned above the model facing down that took photographs after every 0,5mm of displacement. After the experiment was run, the model would be made wet after which the model would be cut and cross-sections would be photographed.

Experiments D1-D7

Experiments D1-D7 aimed at studying the geometry, temporal evolution and distribution of faulting over a listric detachment in an extensional basin scale setting, and how these are affected by implementing variance in parameters such as the initial position of the velocity discontinuity, bulk extension and decoupling.The setup consists of a 30cm wide sheet (purple surface in (*fig. 4)* with one end resting

Figure 3 3D render of the setup used in experiments D1-D7

over a precut wooden block that was fixed to a table. The other end of the plastic sheet was attached to an engine and pulled over the table in the direction indicated by the white arrow (*fig. 4)* During the course of the experiment the wooden block remained stationary relative to the plastic sheet.
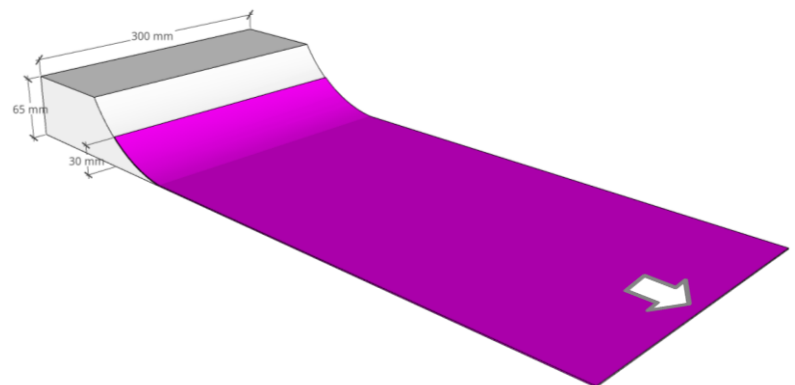
Experiments D8 & D9

The aim of experiments D8 and D9 was to study the effects of differences in layer properties on the development and distribution of thrust sheets in a compressional setting at a crustal scale. Different alternations of quartz sand, glass beads and silicon putty were tested to determine which mechanical stratification produces the most even distribution of thrust sheets. the setup consists of a 30cm wide sheet was pulled under a

Figure 4 3D render of the setup used in experiments D8 and D9

wooden beam (light grey rectangular box in (*fig. 5*) in the direction indicated by the arrow. The wooden beam is fixed to the table and acts as a backstop while a metal bar (dark grey part in *fig. 5*) is fixed to the sheet and acts as a moving barrier that pushed the material towards the wooden backstop. A small lip made of plastic sheet (light blue part in Fig. 2) was attached to the wooden backstop in order to prevent any material from being pushed under the wooden backstop. As in the other experiments, the sides were constrained by metal bars to prevent undesired lateral motion within the model.
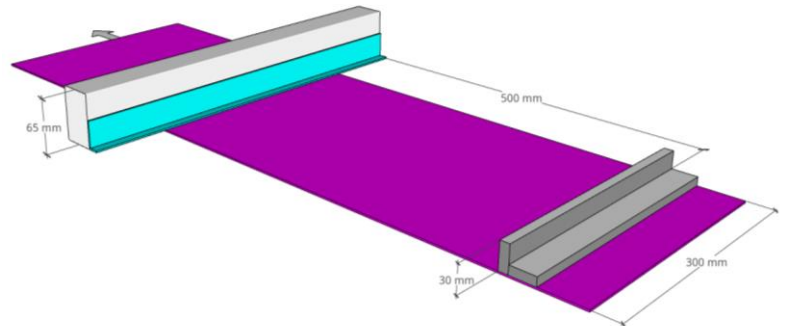
Experiments D10-D12

Experiments D10-D12 aimed at studying the effects of negative inversion of thrust faults at a crustal scale and whether these thrust faults can be reactivated as low angle normal faults. The setup was created to allow for compression and extension in the same model which allows the negative inversion of any thrust sheets that would form. It consisted of three sheets laid on top of each other. The

Figure 5 3D render of the setup used in experiments D10-D12

bottom most sheet (purple surface in (*fig.6*) had a barrier and sandpaper (*beige surface in fig. 6*) attached to it and acted as the main compression mechanism. The sandpaper was added to create a high basal friction in order to promote more localized formation of thrusts. The sheet on top of this (*green in fig. 6*) would move with the
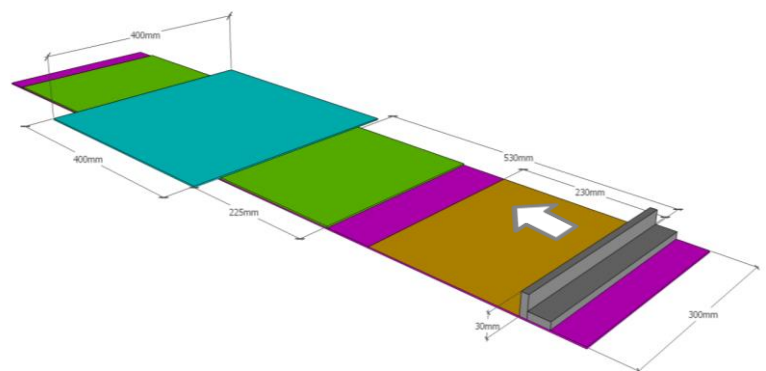
purple sheet during the compression stage while the upper most sheet (*blue in fig.6*) would remain stationary. After the compression phase the purple sheet would remain stationary during which the green and blue sheet would move in the direction indicated by the arrow, thus creating the extension with the aim to reactivate existing thrust sheets during extension.

Experiments D13-D15

Experiments D13-D15 focussed on studying the effects of a brittle ductile interface on the localization of deformation at crustal scale in an extensional setting. The setup of these experiments consisted of a 30cm wide ramp with a twelve-degree angle. One end of a 30cm wide plastic sheet was placed on the ramp in such a way that the end of the sheet would coincide with where the top of the layer of silicon putty terminates against the ramp. The other end of the sheet was attached to an engine and pulled at a constant rate.
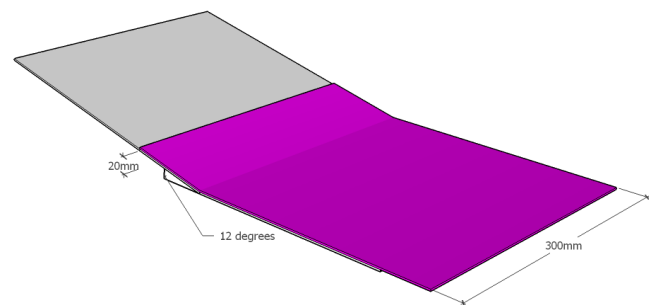

Figure 6 3D render of the setup used in experiments D13-D15

Experiment D16

Experiment D16 is a continuation of the concept of experiments D13-15 and aims to study the effects of excluding a basal sheet on deformation. The setup is analogous to experiments D13-D-15 with the model constructed over a twelve-degree ramp, however D16 had the ramp fixed to a sheet and the ramp was pulled away from the rest of the model instead of the model being placed on top of a plastic sheet that was pulled over the ramp that remained stationary. This was done so that both the layer of silicon putty and the quartz sand made direct contact with the ramp.

4.2 Material properties

Quartz sand
In order to model brittle behavior, quartz sand was used with grainsizes ranging from 63 μm to 355 μm and an average grainsize of 100-300 μm. The mean density (ϱ) is 1500 kg/m3 with a negligible cohesion (C) and an internal friction coefficient (ϕ) of 0,58.

Glass beads
The glass beads consist of microspheres with a grainsize ranging from 200 to 400 μm with a mean density of 2450-2500 kg/m³ (ϱ) and a negligible cohesion (C).

Silicon putty
Silicon putty was used to simulate ductile behavior. The material has a density of 970 kg/m³ and a viscosity (μ) of 5x10⁴ Pa*s.

4.3 Scaling of models

Scaling of dimensions
By deriving the equation of dynamics, two equations can be obtained that form the basis for scaling dimensions, e.g. (Davy and Cobbold, 1991; Smit et al., 2003). In these equations the asterisk identifies the ratios between nature and the model(Brun, 1999).

$$\sigma^* = \rho^* g^* L^* \qquad \textbf{(1)}$$

$$\epsilon^* = g^* (t^*)^2 \qquad \textbf{(2)}$$

Since the densities of rock range from 2300 to 3000 kg/m³ and the densities of the model materials range from 970 to 2500 kg/m³ they are in the same order of magnitude and therefore the density ratio (ρ^*) approximates 1. Since the gravity ratio (g^*) is equal to 1 equation (1) can be simplified to:

$$\sigma^* \approx L^* \qquad \textbf{(3)}$$

This implies that the ratio of stresses (σ^*) must be in the same order of magnitude as the length scale ratio (L^*).

Scaling of material properties

Brittle materials

The brittle deformation of rocks behave according to the Mohr-Coulomb criterion (Byerlee, 1978) which is defined as:

$$\tau = (\tan \Phi)\sigma + C \qquad \textbf{(4)}$$

Where τ is the shear stress, Φ the internal friction angle, σ the normal stress and C the cohesion. Since most crustal rocks have a cohesion of 50 Mpa (Byerlee, 1978), equation (3) in combination with equation (4) shows that with a typical length scale (L^*) of 10^{-6} for analogue models, the cohesion of the material used for analogue models should be negligible. Furthermore, most crustal rocks have an internal friction coefficient (Φ) of around 31°(Byerlee, 1978) which translates to an internal friction coefficient (ϕ) of ~0,60. Quartz sand has a negligible cohesion and an internal friction coefficient of 0,58 and is therefore a correct representation of brittle crustal rocks in analogue models.

Ductile materials

The ductile deformation of rocks can be described by equation (5) (Evans and Goetze, 1979)

$$\dot{\epsilon} = A\, exp(-Q/RT)(\sigma_1 - \sigma_3)^n \qquad \textbf{(5)}$$

Where $\dot{\epsilon}$ is the deviatoric strain rate, Q is the activation energy, R the universal gas constant, T the absolute temperature, A is a material constant and n the stress exponent. Silicon putty is used to model the ductile behavior of lower crustal rocks. Silicon putty is a Newtonian viscous fluid with a stress exponent of n≈1 , which means that its resistance to flow is linearly dependent on the strain rate. Experimental data suggest that most natural ductile rocks have stress exponents between 1 and 4 (Smit, 2005). Lower ductile crust has a stress exponent of ≈ 1 while upper mantle rocks have higher stress exponents. Since we are only interested in modelling the properties of lower ductile crust, silicon putty with Newtonian viscous properties is an excellent substitute for these types of natural rocks in the models presented in this study. The shear strain rate ($\dot{\gamma}$) is described by the equation:

$$\dot{\gamma} = \frac{V}{T_d} \qquad \textbf{(6)}$$

Where V is the rate of displacement and T_d the total thickness of the ductile layer. Since $\sigma^1 - \sigma^3 = 2\tau$ the shear stress can be written as:

$$\tau = \frac{\eta V}{T_d} \qquad \text{(7)}$$

or:

$$\tau = \eta \dot{\epsilon} \qquad \text{(8)}$$

This implies that the strength of the ductile layer decreases with increasing thickness. Another important relation that can be obtained from equations (7) and (8) is that the strength of the ductile layer also depends on the rate of displacement and since the range in viscosities of silicon putty is limited, this can be compensated by adopting different rates of displacement.

4.4 Strength and limitations of (analogue) models

Any model is a simplification of the complexity of natural occurring processes in geology. Herein lies their strength because it allows us to study the role of individual parameters. The inherent danger is that the limitation of the materials available for analogue models leads to an oversimplification of the true range of properties of different rocks in nature. For example, in this study quartz sand is used as a general substitute for the behavior of rocks and does not take into account the different mechanical properties of the variation in sedimentary rocks. Another major difference is the rates at which the models are deformed in this study are kept at a constant value while in nature the rate of extension and compression can vary over time.

It is however important to note that although analogue models pose some limitations they are a very powerful tool in geology. Analogue models or any model for that matter allow the systematic testing of variance in parameters in a controlled tangible environment. The concept of analogue modelling is not to be a fully accurate representation of nature, but rather to test certain concepts found in geology and being able to extrapolate these findings to nature. Furthermore, one of the most powerful properties of analogue models is that they span four dimensions compared to three in nature. In nature one can only observe the current state of structures while in analogue models the evolution of these structures over time can be observed and studied.

5. Experimental results

During the experimental part a total of 16 analogue tectonic modelling experiments were constructed and run. This section however only describes 14 runs since four experiments, namely D2, D3, D13 and D15 experienced issues with either high sidewall or leaking of silicon putty during construction. These experiments are therefore not described in this section since their results were not usable.

5.1 Basin scale extension

These experiments aimed at testing the effects of a predetermined listric detachment on the evolution and distribution of faulting on a basin scale. All experiments involved applying extension over this listric detachment that represents the Coffee Soil Fault that bounds the Dutch Central Graben to the east. Experiments were conducted with only brittle models and one model with a 1cm layer of putty at the bottom to simulate a ductile detachment.

Experiment D1

The overall geometry of experiment D1 is that off a roll-over anticline with a crestal collapse graben. These structures formed during a bulk extension of 50mm. In the first stages the extension is accommodated by the detachment fault D1 that accommodates most deformation as indicated by the larger volumes of pink, black and yellow sediment fill. During deformation a series of angle normal faults form at angles ~65°. Due to rotation the faults nearest to detachment D1 show angles greater (*N5, N6*) or less than (*N7*) 65°. After 45mm of bulk extension, movement along detachment D1 halts and fault N7 accommodates the remainder of the bulk extension (*fig. 9C*). The faults antithetic to D1 show significantly less displacement resulting in tilting of the basement strata and in wedge-shaped sedimentary infills. The basement strata show progressive tilting towards the detachment D1 creating an overall roll-over geometry. The crestal collapse graben which is comprised of faults N1-N4 starts to form at roughly 50% bulk extension with the activation of fault N2.
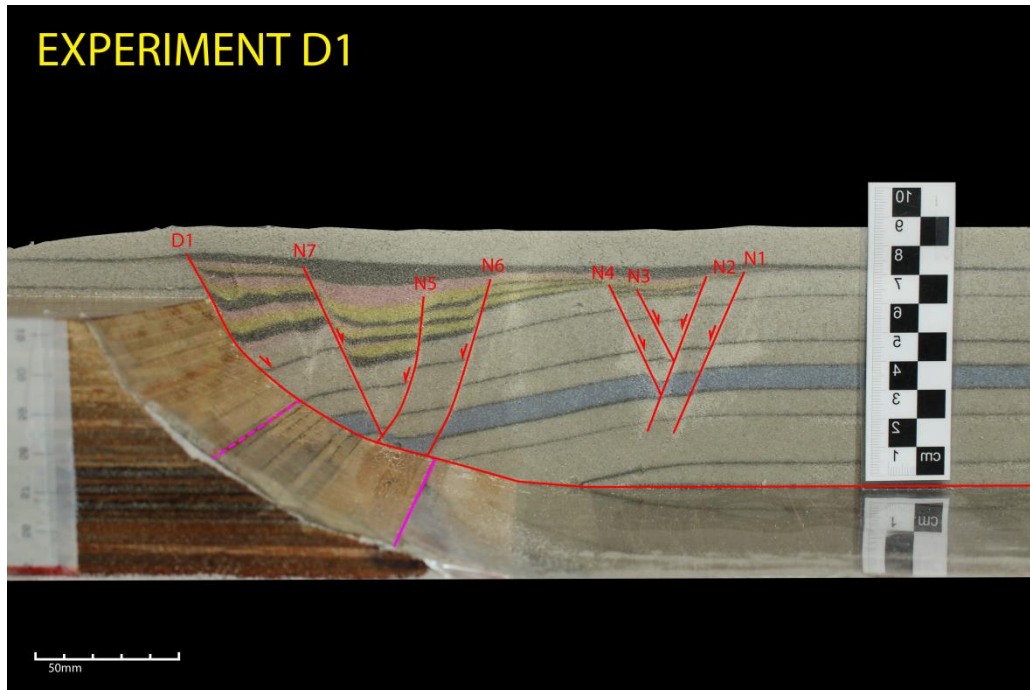
Figure 7 Cross section of D1 showing asymmetric normal faulting producing wedge shaped sedimentary infills. The majority of extension and deformation took place along detachment D1. Note the overall rollover-like geometry of basement and sediment fill. The purple lines indicate the initial and final position of the basal sheet.
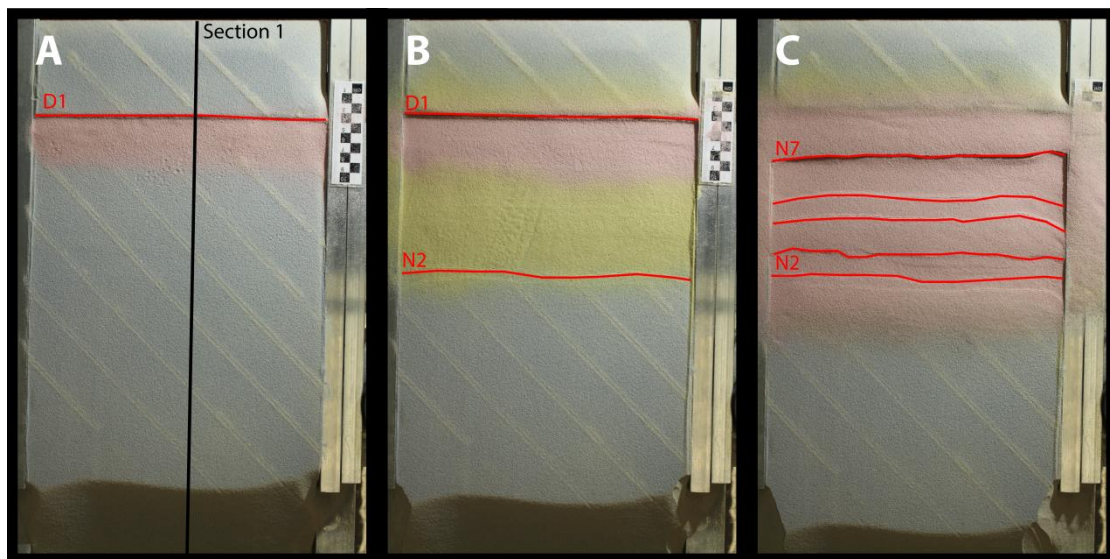

Figure 8 Topviews A,B and C at 20%, 50% and 100% bulk extension. Note that accommodation of displacement is transferred from D1 to N7 between B and which occurred at 90% bulk extension.

Experiment D4

Experiment D4 is identical in setup to D1 except for the lower initial position of the basal sheet with respect to the surface. With the basal sheet at a lower position (*10mm vertical distance*) the majority of deformation is concentrated around the edge of the basal sheet and the path it followed along the listric block. The structures that developed are mainly high angle normal faults (65%) dipping away from the ramp, along with antithetic high angle normal faults producing a series blocks and grabens that show progressive tilting towards the proximal part of the model similar to D1. The final deformation shows a roll-over geometry dipping towards the listric block.
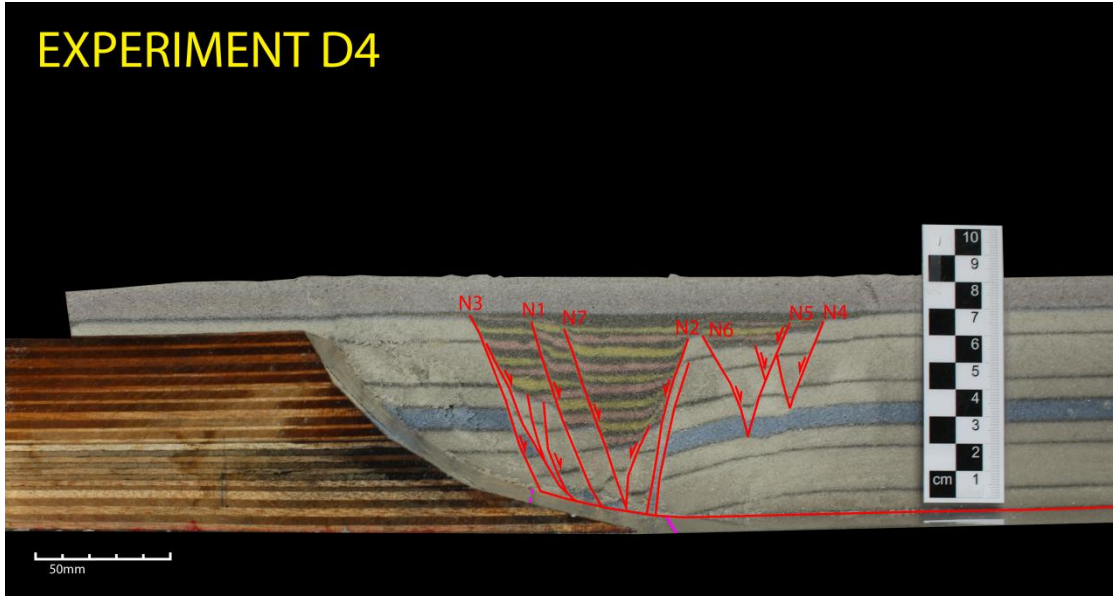
Figure 10 Cross-section of experiment D4 with a lower initial position of the basal sheet showing the formation of high angle normal faults at ~65°. Note the detachment fault deflecting upward at the initial basal sheet position.
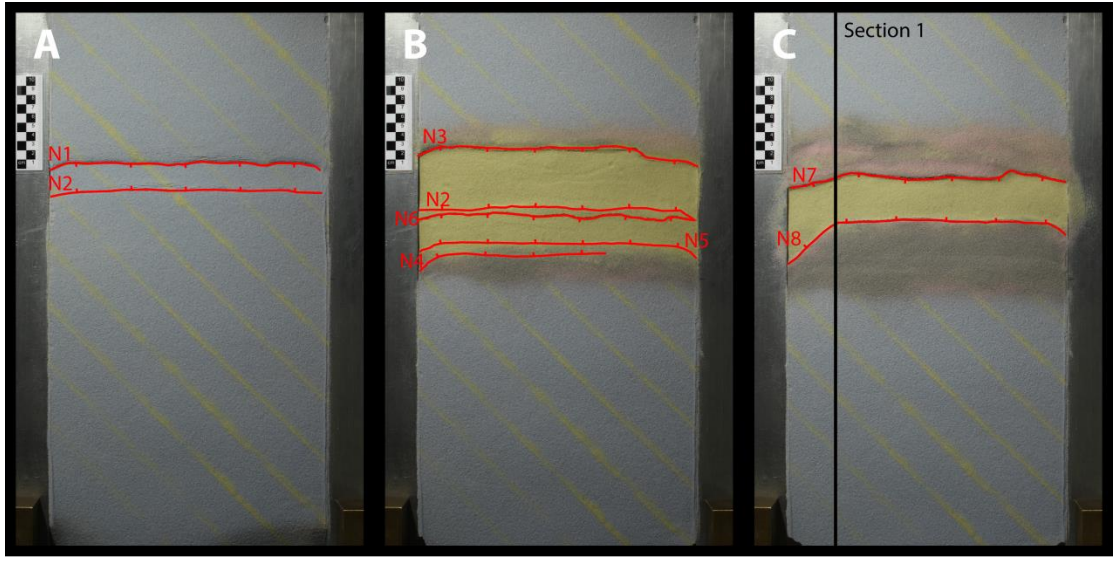

Figure 11 Topviews A, B and C of experiment D4 at 10%, 70% and 90% bulk extension.

Experiment D5

The overall geometry of experiment D5 is that of a roll-over anticline with a crestal collapse graben. During the course of the experiment a total of four faults have been produced with indication of the initiation of fault activation in the roll-over. The two antithetic faults in the most distal part of the model seem to terminate at an approximate height of 20mm from the base of the model.
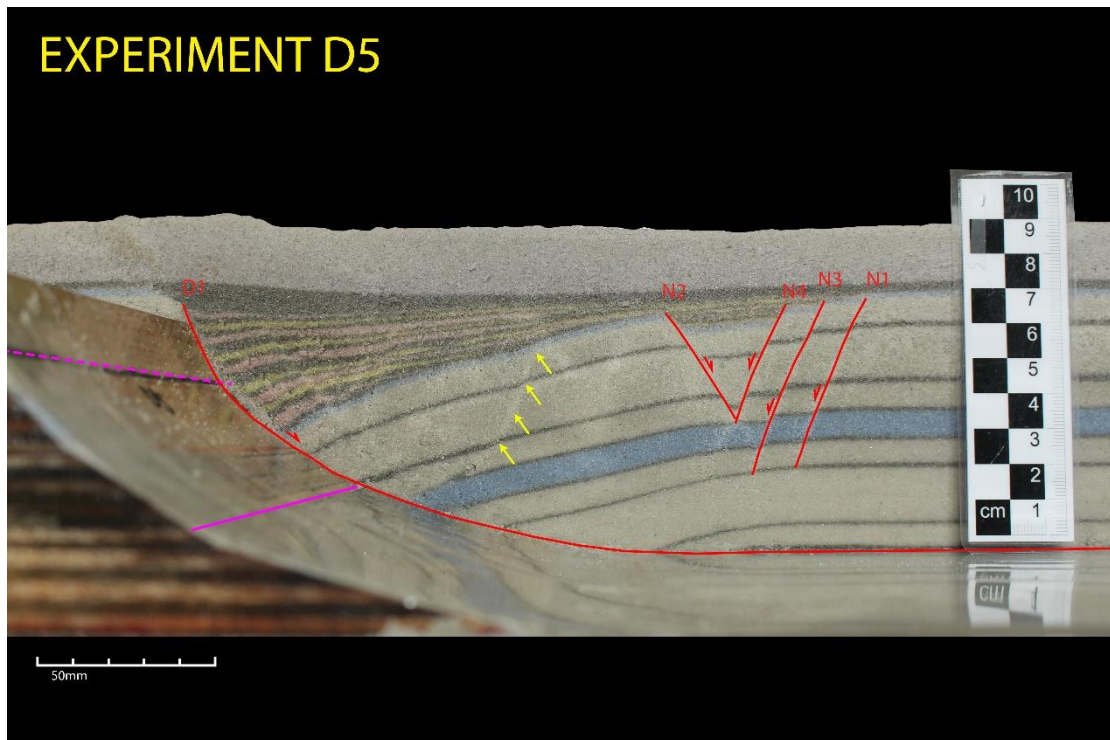
Figure 12 Cross-section of experiment D5 showing an overall roll-over anticline geometry with a crestal collapse in the distal part of the experiment. Yellow arrows mark early markings of onset of faulting.
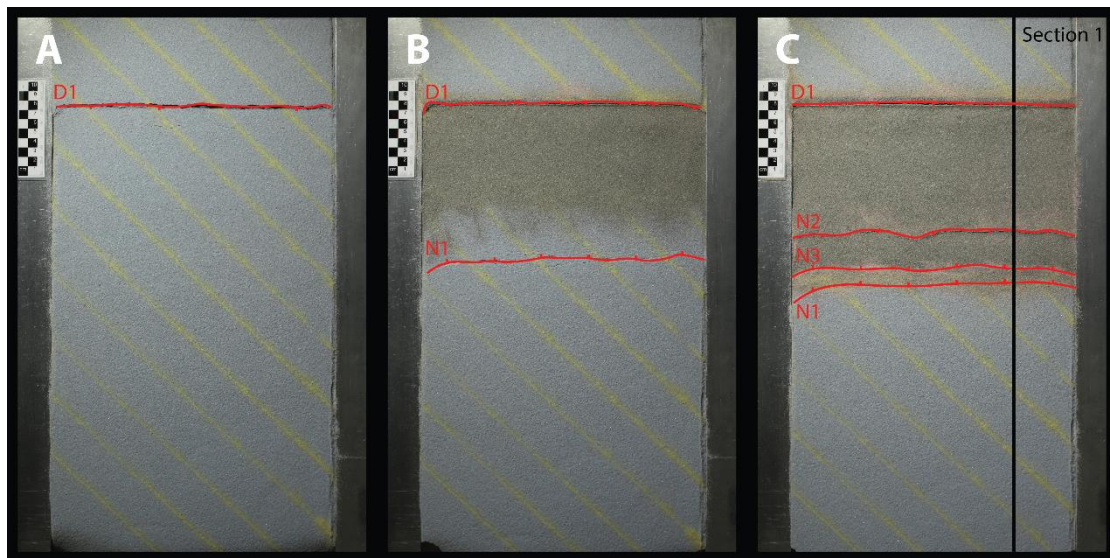

Figure 93 Topviews A, B and C at 10%, 25% and 90% bulk extension.

Experiment D7

Experiment D7 has the same setup as D1 both in terms of construction and initial position of the basal sheet but in this case only 2.5cm of bulk extension was applied. The overall geometry produced during this experiment is that of a roll-over anticlinal structure with early indications of crestal collapse faults started to form in the more distal part of the experiment where the sedimentary wedge thins out.
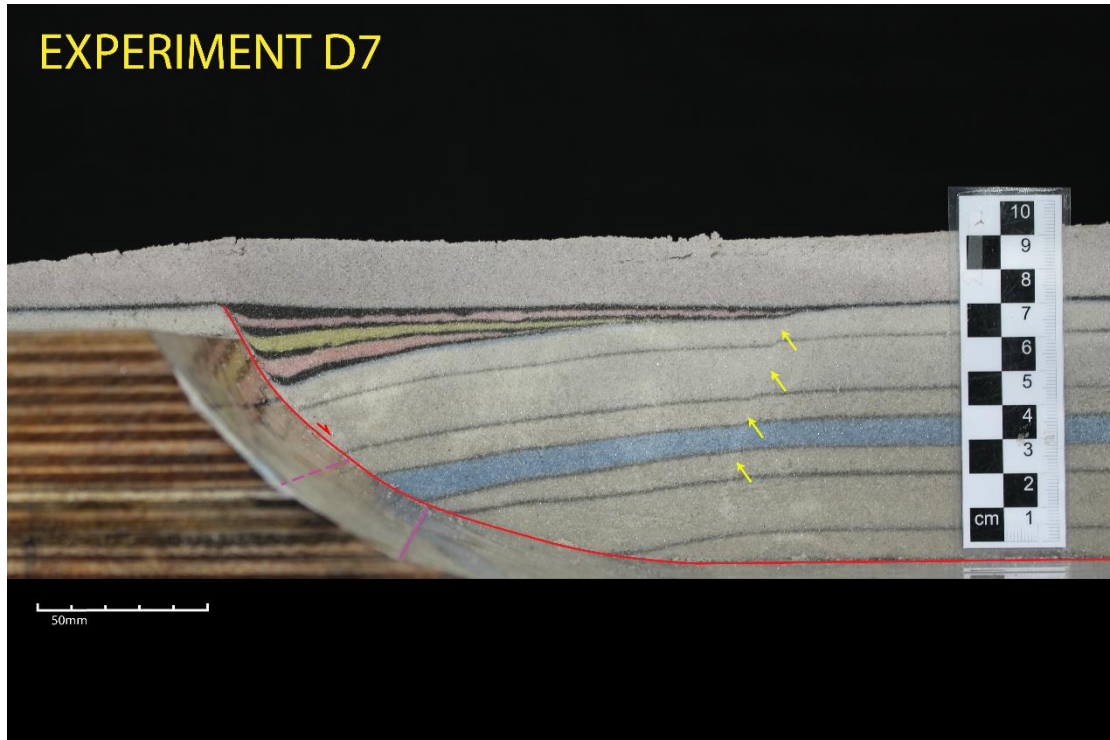

Figure 14 Cross-section of experiment D7 showing an overall roll-over anticline geometry with bright lines in the sand indicating the formation of a crestal collapse marked by the yellow arrows.

Experiment D6

Experiment D6 was deformed without metal sidebars, removing any sidewall friction and consequently eliminating any decoupling between the quartz sand and silicon putty. The cross-section shows a strong similarity to that of D1 (*fig. 8*) with high angle normal faults forming at ~65° with faults being rotated passively close to the ramp due to the strata being tilted. This progressive tilting towards the ramp again shows an overall roll-over anticline geometry.
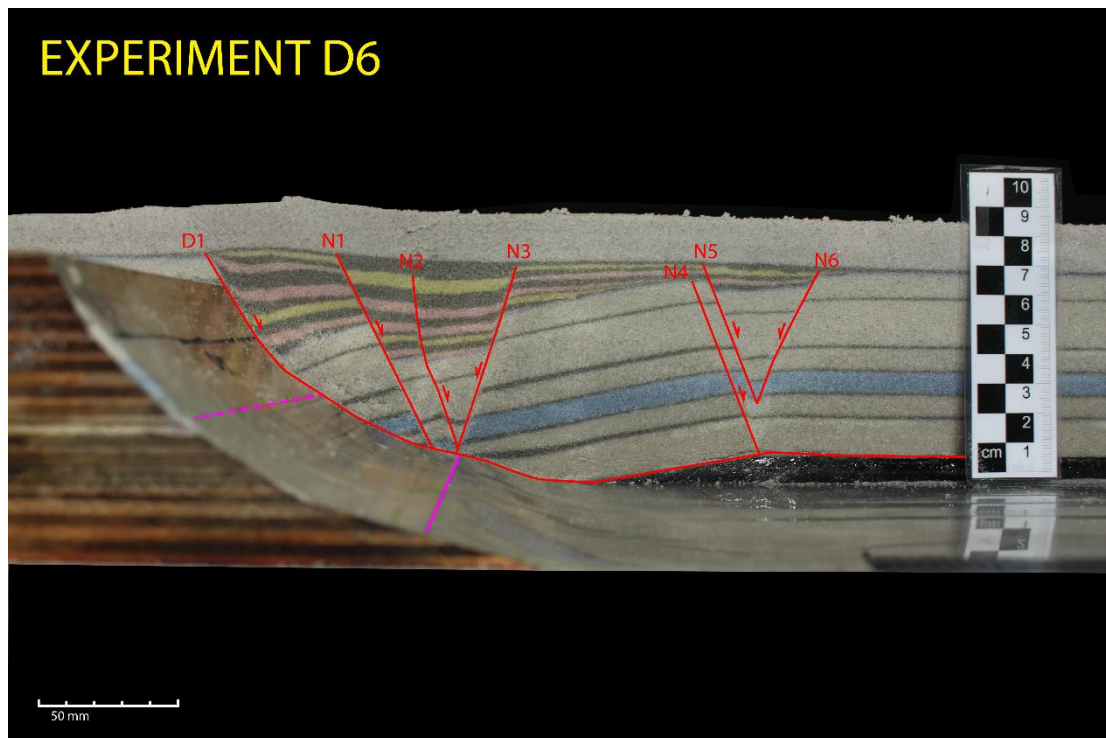

Figure 15 Experimental setup similar to D1 but with 1cm of silicon putty at the base showing similar development of structures most noticeably the distribution of faults and the overall rollover geometry.

During extension initial deformation was accommodated by detachment D1 along which the largest displacement occurred. At 50% bulk extension fault N1 started to develop nearly concurrent with the development of fault N2 producing a crestal collapse graben. This conjugate set of faults remained active up until the end of extension however, displacement along N1 temporarily halted at 85% bulk extension, the same time when displacement at D1 stops and D5 became the most active.
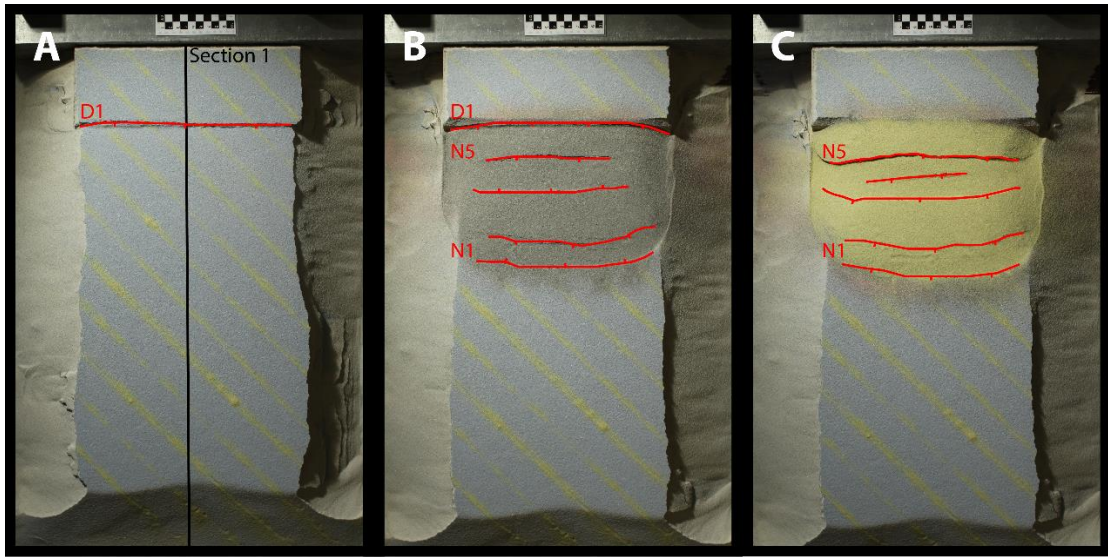
Figure 16 Topviews A,B and C at 10%, 77% and 100% bulk extension. Note that accommodation of displacement is transferred from D1 to N5 between B and which occurred at 85% bulk extension.

5.2 Crustal scale experiments

These aim of these experiments was to test the effects of the structural grain below the Dutch Central Graben on the development and placement of the basin on a crustal scale.

Experiment D14

Experiment D14 had the same setup as that of D13, however, in this case the sidewalls of the experiment moved with the basal sheet, eliminating any sidewall friction. This resulted in the development of three normal faults over the ramp at the junction of the layer of silicon putty and basal sheet. At 30% of bulk extension fault N1 started to develop (*fig. 18A*) shortly after which the antithetic fault N2 started to develop at 70% of bulk extension, resulting in a graben structure to develop (*fig. 19B*). At 95% of bulk extension fault N3 started to develop internally in the depressed block in the graben structure (*fig. 18C*) . The block between faults N1 and N3 in the graben structure shows tilting towards the left side of the model (*fig. 17*). Furthermore, the layers right of fault N2 also show tilting towards the left, indicated by the blue dotted lines (*fig. 12*).
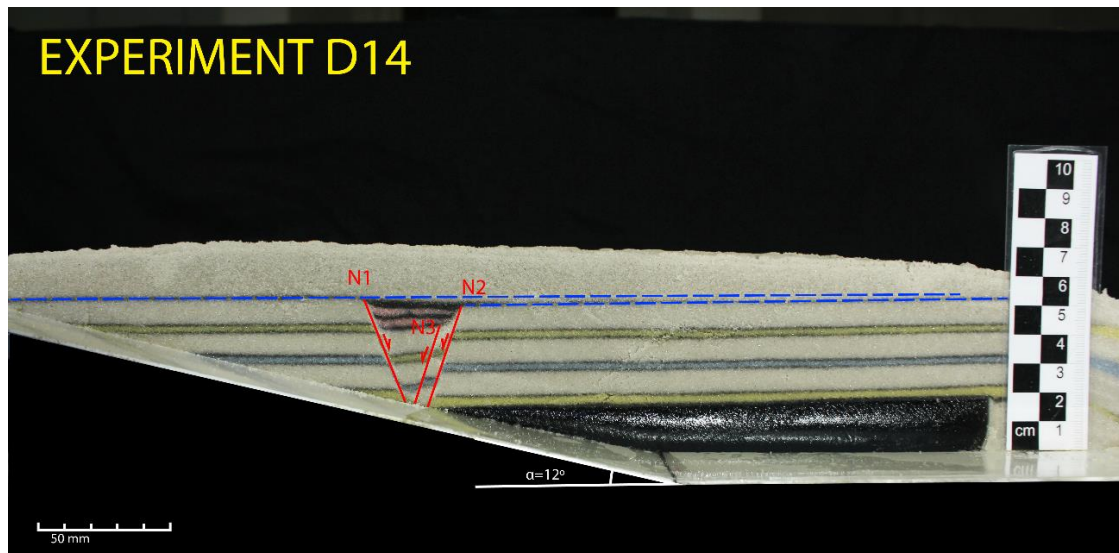

Figure 17 Cross-section experiment D14 showing development of an asymmetric graben structure and tilting of the strata during deformation indicated by the blue lines. Note the more prominent tilting in the depressed block between the conjugate set of faults producing an overall roll-over geometry.
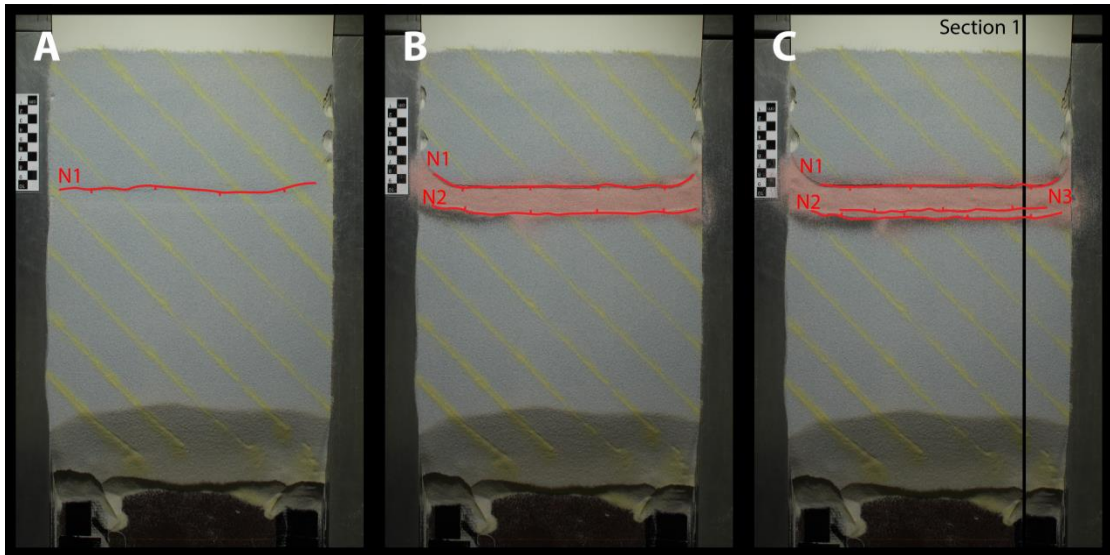
Figure 18 Topviews A,B and C at 30%, 70% and 95% bulk extension respectively.

Experiment D16

Experiment D16 had a similar setup in terms of geometry but differs in mechanics from D14 in the sense that the ramp was moved away underneath the model instead of the model being moved over the ramp along a plastic sheet. The overall geometry formed is that of a graben with smaller antithetic faults internally located in the depressed graben block. Deformation is focused at the location where the brittle-ductile contact meets the ramp.
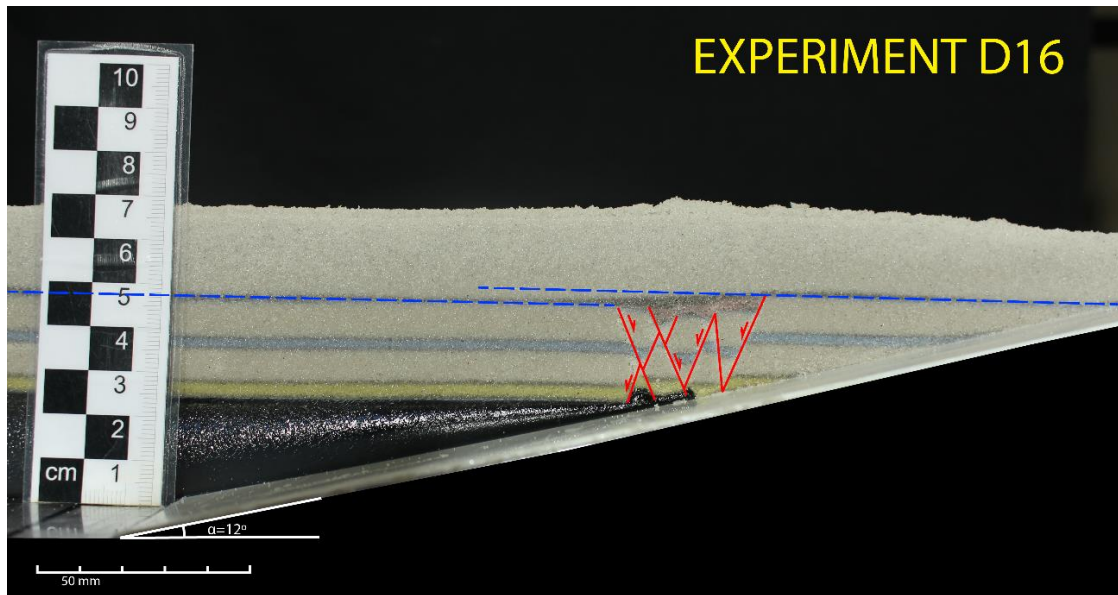

Figure 19 Cross-section of experiment D16 showing conjugate fault structures developing at the contact between ductile layer and ramp. Note the absence of the plastic basal sheet.
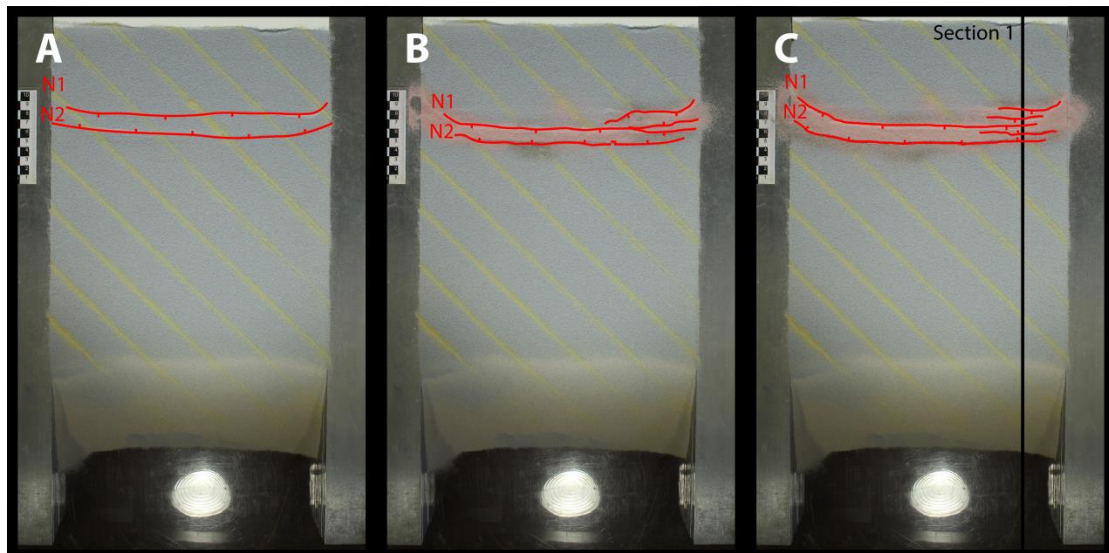

Figure 20 Topviews A, B and C of experiment D16 at 25%, 65% and 100% bulk extension respectively.

5.3 Extensional reactivation of thrust sheets

These experiments where performed in order to see if it is possible to reactivate a thrust sheet as a low angle normal fault.

5.3.1 Brittle

Experiment D8
D8a

Deformation initiated with the formation of the pop-up geometry in the more proximal part relative to the wooden backstop. This structure continued to grow while forming a 2nd forethrust T3 in sequence after which a second pop-up geometry formed in the distal part of the experiment. Faults T5 and T6 envelop the original 2nd pop-up geometry with T4 being developed last, which eventually crosscuts T3.

D8b

Unlike D8a or D8c this experiment experienced considerable boundary effect which is likely to be caused by the stronger sidewalls due to it being flanked by the two other models. The cross-section is therefore positioned in the centre of the model to exclude these boundary effects. The results show a significant difference in geometries when compared to D8a and D8c. Faults T1-T4 are part of the first major structure formed. These thrusts formed in sequence with T1 being formed first and T4 last. Thrust faults T5 and T6 are part of a pop-up geometry that formed during the final stages of the experiment. These faults show less offset compared to T1-T4. Fault T4 was the last of these faults to be active up until the point T5 and T6 started to form so deformation was transferred from the thrust stack to the pop-up geometry.

D8c

Experiment D8c produced similar results to experiment D8a (*fig 21*) with a pop-up geometry in the distal part of the model in the initial stages of the experiment with a progression of thrusting radiating from this central pop-up both towards the hinter and foreland. At 72% of bulk shortening a faults T5 and T6 became active forming a pop-up geometry. This second pop-up accommodated all deformation in the last 28% of bulk shortening resulting faults T1-T5 to become inactive during this stage.
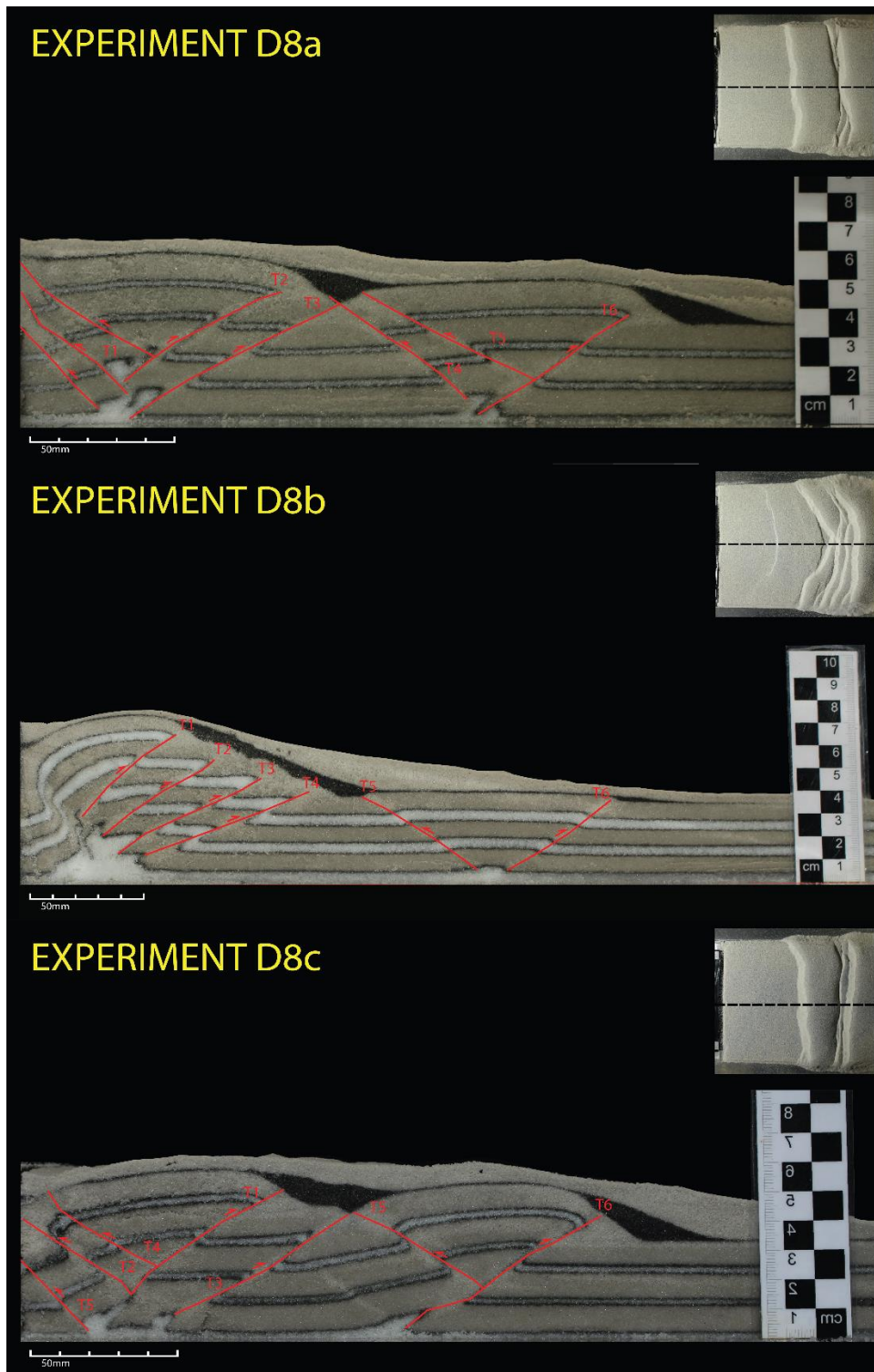
Figure 21 Top Panel: Cross-section of experiment D8a showing two pop-up geometries. Setup has an alternation of layers glass beads (2mm) and quartz sand (8mm), where the glass beads layers are 5cm shorter than the quartz sand layers. Black dotted line in topview marks location of cross-section. Middle Panel: Cross-section of experiment D8b showing stacking of thrust faults in the proximal part and a pop-up geometry with relatively small offset in the distal part. Stacked thrusts show a sense of motion towards the foreland. Deformation is more concentrated near the backstop in the central part of the model. Setup uses alternating layers of glass beads (4mm) and quartz sand (6mm). Bottom Panel: Cross-section of experiment D8c showing similar results to D8a with two main pop-up geometries. Layering is identical to D8a except for the glass beads layers equally long to the quartz sand layers.

27

5.2.2 Ductile

Experiment D9

Experiment D9 resulted in a relative high amount of localized deformation near the moving wall resulting in the development of a fault-bend fold as the main structure. This structure was the first to form during the run of the experiment. At 70% of bulk shortening this fault-bend fold developed to a size where the back limb of the fold started to envelop the moving wall and create an almost horizontal thrust opposite in the direction of shortening. To prevent this from continuing, at 70% of bulk shorting, sand was added to effectively increase the height of the moving wall. At 90% of bulk shortening the low offset thrust fault in the distal part started to develop and accommodated only a small amount of the last 10% of the bulk shortening since the fault-bend fold was still active during this last stage (*fig. 23*).
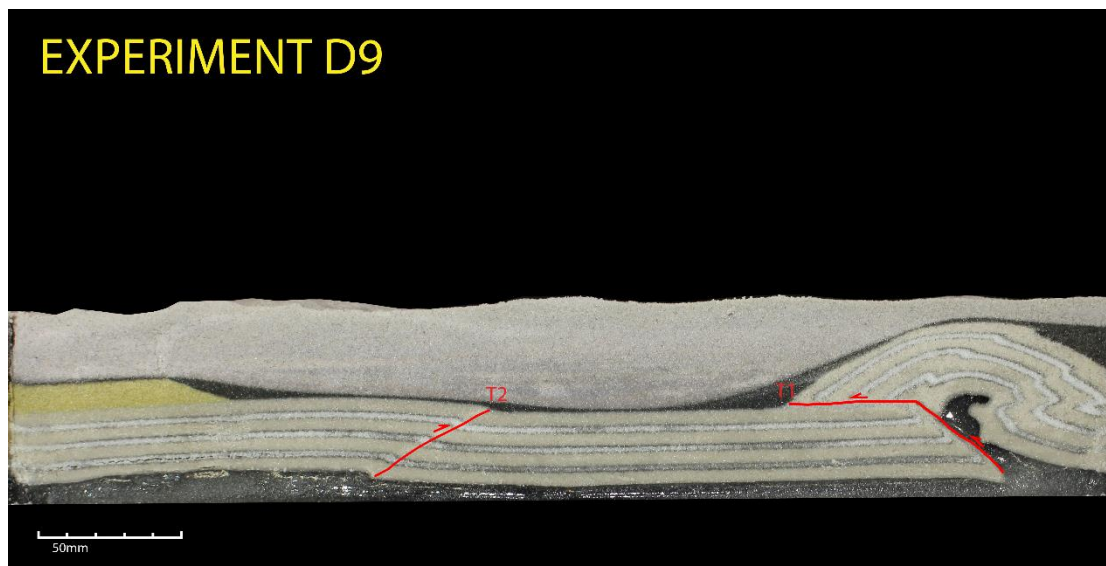

Figure 22 Cross-section of experiment D9 showing the formation of a fault-bend fold with internal micro-faults and a low offset thrust fault in the proximal part. Note the 10mm addition of yellow sand near the backstop.
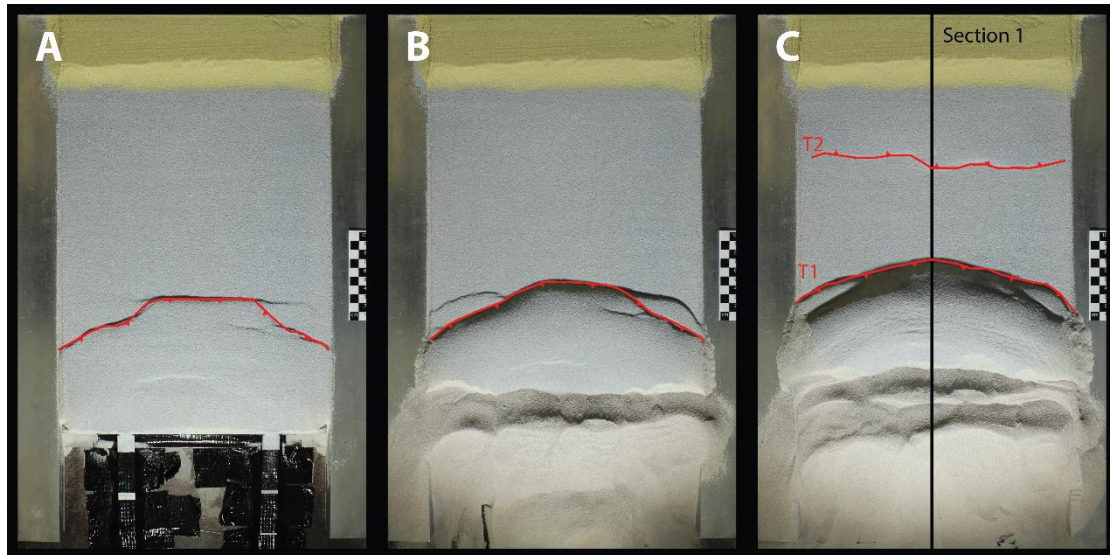
Figure 23 Topviews A, B and C at 15%, 70% and 90% bulk compression with a single thrust forming during the course of the experiment, during the final stage of the experiment thrust T2 becomes active.

Experiment D10

Compression phase

Experiment D10 successfully shows the reactivation of a thrust fault during extension. This thrust fault R1 was created during the compression phase where during the first phase of compression a thrust wedge is being created at the boundary between the static and moving plastic sheets. This thrust wedge internally develops 5 small folds, each developing in sequence after which the development of the thrust wedge halts and a series of larger thrust complex start developing, which prograde in sequence to the foreland (*fig. 24*). R1, the reactivated surface is the second to last of these thrusts to develop before the total amount of compression is reached. A total of 5 forward thrusts have developed during compression with the last one showing a very clear example of a ramp/flat geometry.
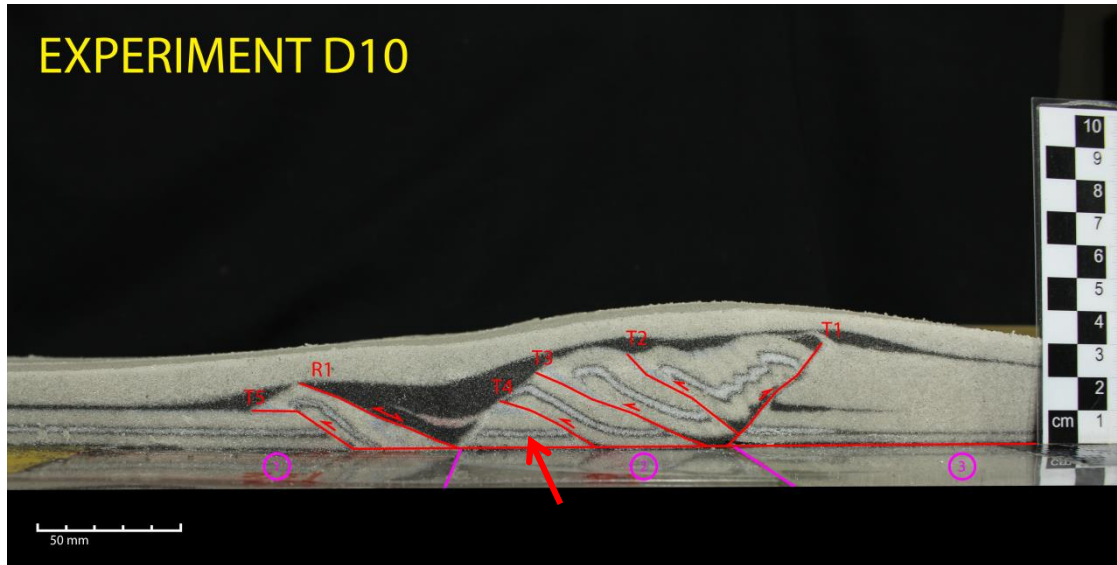
Figure 104 Cross-section of experiment D10 showing a thrust wedge to the right and a thrust duplex to the left. R1 shows negative inversion of a thrust fault during the extension phase. The block indicated by the red arrow rests in a horizontal position but was initially oriented parallel to the fault R1. Note that the black sand situated above the pink lens was added after the experiment finished to preserve the geometry of the structures formed.
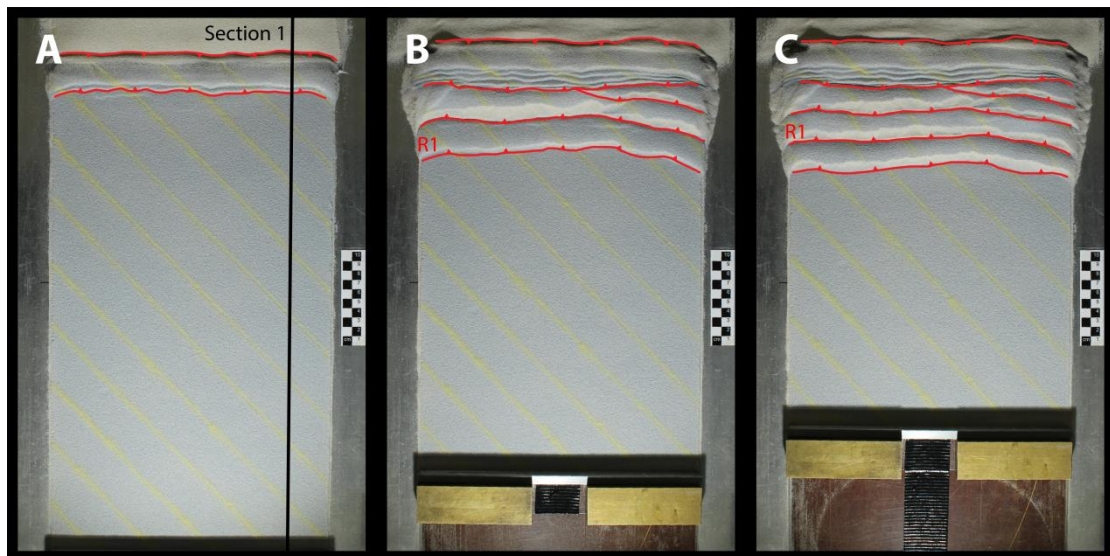

Figure 25 Topviews A,B and C at 12%, 70% and 100% bulk compression respectively showing in sequence thrusting. Note the thrust wedge remaining largely undeformed between B and C as this localized deformation is transferred to more delocalized deformation in the propagation of thrusts away from the wedge.

Extension phase

During extension most of the deformation was accommodated by the reactivation of thrust fault R1. This extension placed the block indicated by the red arrow in figure 5 along fault R1 from a tilted position parallel to fault R1 to a completely horizontal position at the end of the bulk extension. The rest of the topography and structures developed during the compression phase remain intact during extension.
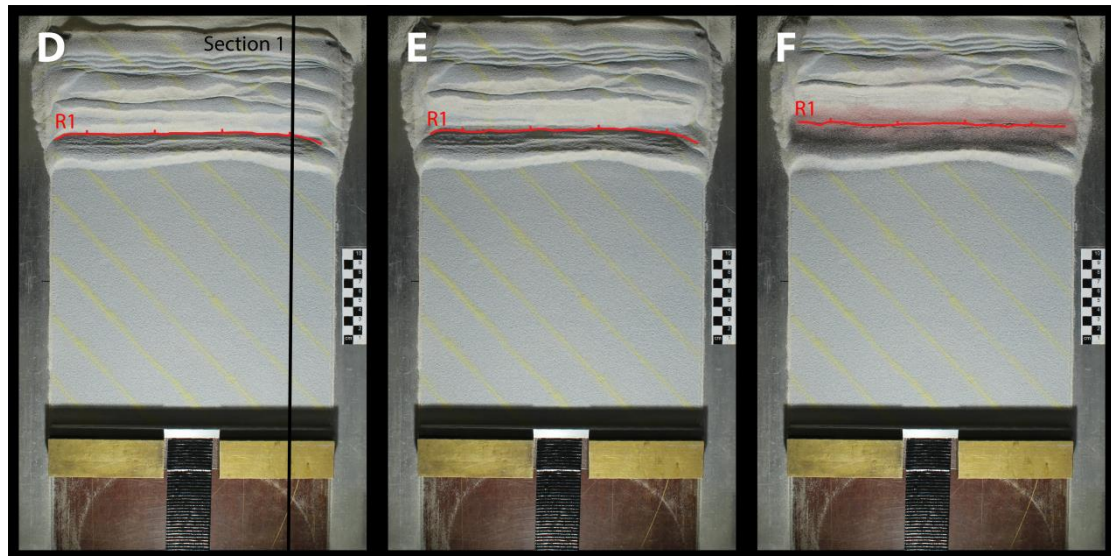

Figure 26 Topviews D,E and F at 42%, 72% and 100% bulk extension respectively, showing negative inversion of the thrust fault R1 which accommodates most of the deformation.

Experiment D11

Compression phase

After 15cm of bulk compression an overall geometry of a thrust duplex was formed comprised of two thrust faults developing in sequence. The first thrust T1 formed concurrently with the antithetic thrust T2 effectively creating a pop-up structure in the initial stages of compression. To further promote the development of thrusting towards the foreland (*left in fig. 27*) additional sand was placed over thrust fault T2. After 52% bulk compression a second thrust T3 started to develop again with an antithetic thrust T4 that cannot be observed in the cross-section (*fig. 27*) but can be seen in the topview images of the model (*fig. 28).* These topviews also show that once this second structure starts to develop thrust T2 becomes inactive but becomes reactivated once the second thrust duplex converges with the thrust duplex associated with fault T2.
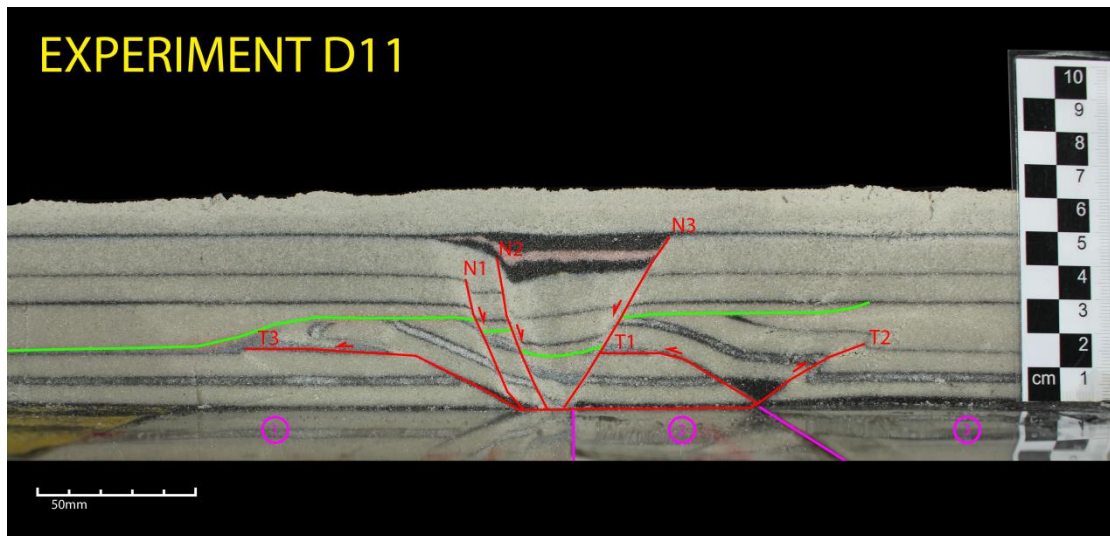
Figure 11 Cross-section of experiment D11 where first 15cm of bulk compression was applied after which the majority of topography was removed before applying 3cm of bulk extension. Green line marks surface after topography was removed. Note that the structures formed in the compressional phase seem to have no effect on the development of structures in the extension phase.
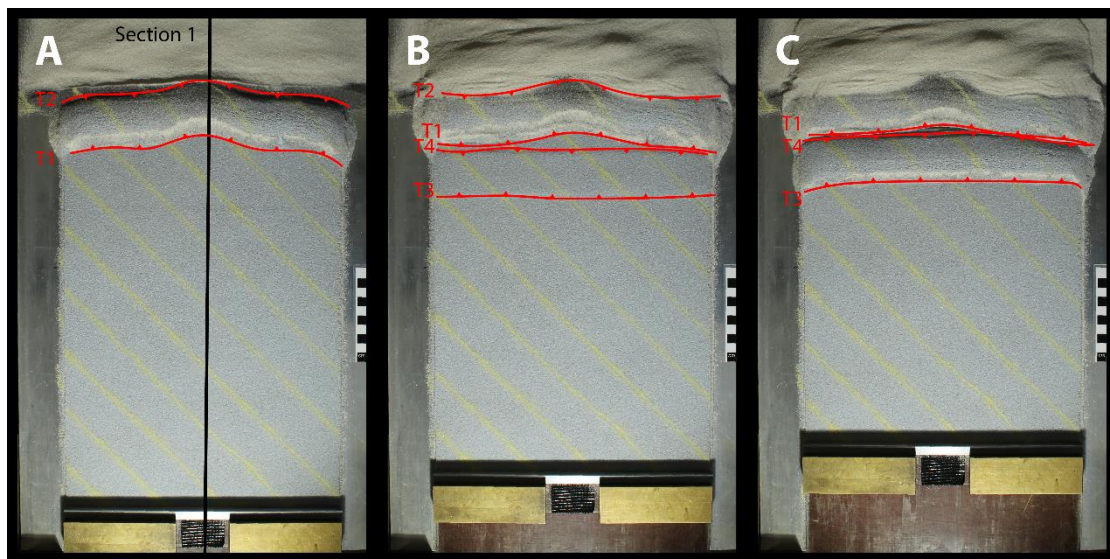
Figure 2812 Topviews A,B and C at 25%, 50% and 100% respectively showing the formation of thrust T3 with antithetic thrust T4 at 50% when T1 and T2 become inactive.

Extension phase

After the compression phase the topography was eroded to 9mm above the original starting thickness of 14 millimeters. Afterwards, additional sand was added to create a total model thickness of 50mm after which extension was applied. Extension resulted in the formation of three normal faults N1, N2 and N3. N2 and N3 are antithetic in relation to each other and converge at the boundary between sheet '1'

and '2'. The overall geometry produced is that of a graben structure with the graben between faults N2 and N3 showing tilting towards the foreland.

The extension was not accommodated by any of the thrusts faults formed during the compression stage and faulting in the extension phase seems unaffected by any of the structures formed in the compression phase.

Experiment D12

Compression phase

During the compression phase a single thrust T1 developed and accommodated all of the 6.2cm bulk compression. During the course of the experiment any topography that developed was removed by scraping it off. The thrust fault developed at the margin between sheet '2' and sheet '1' (*fig. 29*).

Extension phase

After the compression phase 12mm of black and yellow sand was added before 1cm of bulk extension was applied to the system. This resulted in the formation of two normal faults N1 and N2 that are antithetic and produce a single graben. The faults N1 and N2 converge at the boundary between sheet '1' and sheet '2' where the thrust T1 developed as well. However, during extension any of the structures that have developed seem to be unaffected by thrust fault T1.
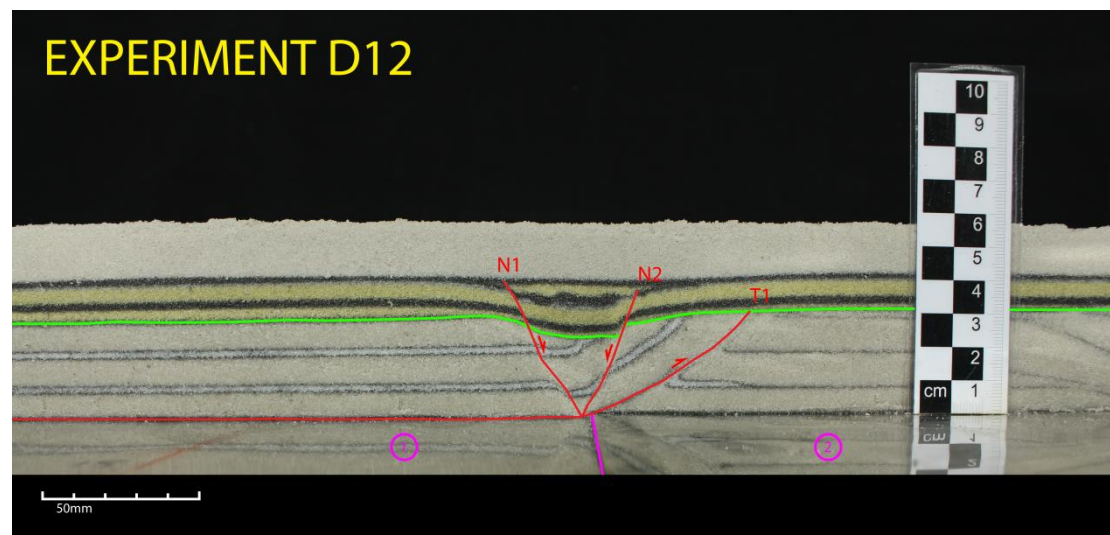

Figure 29 Cross-section of experiment D12 where first 6.2cm of bulk compression was applied during which topography was removed. After compression 12mm of quartz sand was added (black and yellow) before applying 1.0cm of bulk extension. Note the single thrust developed at the edge of sheet '1'. Faulting during extension appears to have not been affected by the thrust fault.

6. Discussion

6.1 Dutch Central Graben basin geometries

The first seven experiments D1-D7 aimed at reconstructing the effects of a listric shaped detachment surface on the distribution and geometry on a basin scale setting. In addition experiments D2,D3 and D6 incorporated the use of a 1cm layer of silicon putty at the bottom of the experiment to study the effects of a ductile detachment on the fault distribution and geometry. The experiments were constructed using a basal sheet on which the experiment rested, positioned over a listric shaped block that acted as a detachment surface during the run of the experiment. The listric shape of the detachment was modeled after the geometry of the Coffee Soil Fault that bounds the Dutch Central Graben to the East (Lyngsie and Thybo, 2007). These seven experiments are therefore based on the assumption that the listric shaped detachment that is associated with the Coffee Soil Fault was a pre-existing structure present in the crust.

From these experiments the most striking results obtained, are those from D1, D4 and D6. D1 and D6 show that when extension is applied over a listric detachment, structures develop similar to those interpreted from the MONA LISA-3 profile FIG! (Mona Lisa Working Group, 1997b; Lyngsie and Thybo, 2007; Smit et al., 2016). Both D1 and D6 (*fig. 30*) show the development of two sets of faults, one in the roll-over anticlinal structure and one set associated with a crestal collapse structure. These two sets of faults are separated by a relatively large structure with a higher elevation that is reminiscent of the mid –graben high discussed by (Lyngsie and Thybo, 2007) and shown in figure 31.

The cross-section of D4 (*fig. 30)* shows similar structures developing to that of D1 and D6 but deformation is more localized and although a mid-graben high develops,
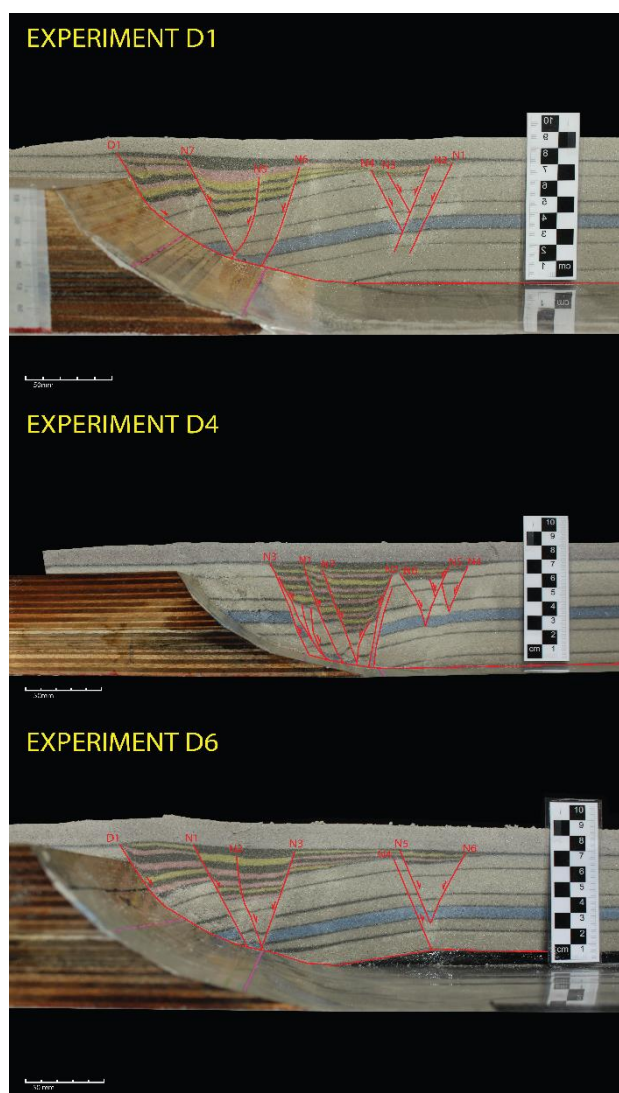

Figure 30 Cross sections for experiments D1, D4 and D6

the overall horizontal scale of the structures is significantly smaller when compared to the cross-sections of D1 and D6 (*fig. 30*) This shows that the initial position of the basal sheet and thus the initial geometry of the detachment has large implications on the geometry of the system and since the geometries produced in experiments D1 and D6 strongly resemble those found in the Central Graben it can be assumed that the detachment geometry and position of the basal sheet in these experiments are indicative of the detachment over which the Central Graben formed.
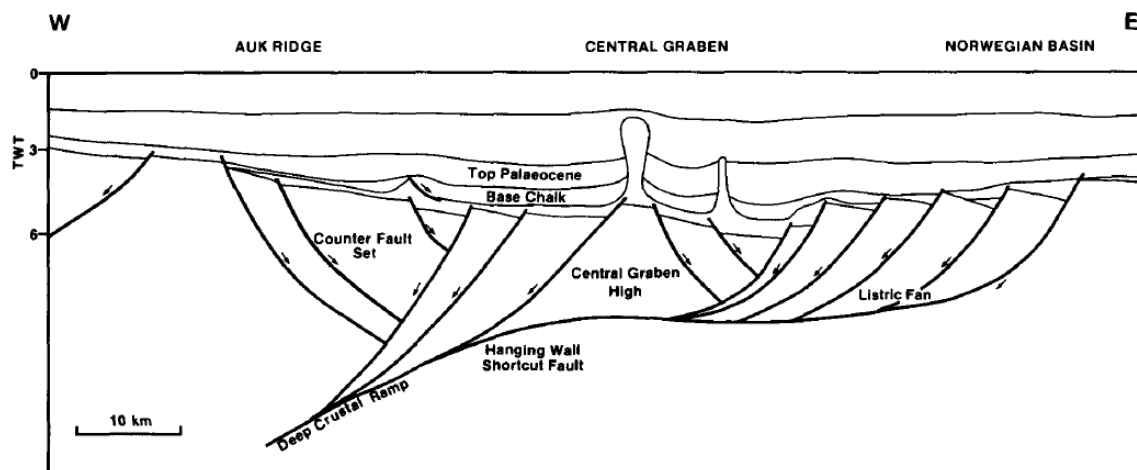

Figure 3113 Crustal model of the Central Graben developing over a listric detachment with a mid-graben high. Adopted from (Gibbs, 1984)

6.2 Reactivation of Paleozoic structures

Following Smit et al., 2016, it can be assumed that the collapsed accretionary complex is still present between Avalonia and Baltica. To test the effects on the formation of the Central Graben, attention was focused on the extensional reactivation of Caledonian thrust sheets with experiments D8-D12. Based on previous experimental studies (Colletta et al., 1991; Graveleau et al., 2012), an alternation of glass beads and quartz sand was chosen to create anisotropy in the material and promote the formation of thrust sheet towards the foreland through layer parallel sliding. Results from experiment 8 show (*fig. 21*) that different ratios of thickness between the quartz sand and glass beads produce a significant difference in geometries. D8b, with an alternation of 6mm of quartz sand and 2mm of glass beads (*fig. 21*) produced more forward thrusts when compared to D8a and D8c. Thus a larger ratio in thickness of glass bead layers compared to quartz sand is more susceptible to producing forward thrusts.

The significance of promotion of forward thrusts is based on the tectonic relation between Baltica and Avalonia where the latter has been thrust over Baltica creating

the Caledonian accretionary wedge (Smit et al., 2016) In such an accretionary wedge, thrusting will be oriented in the direction of the foreland in this case Baltica. It is therefore possible that a large fore-thrust associated with this accretionary complex has been reactivated as the detachment for the Dutch Central Graben. Which is supported by the results from experiment D10 (*fig. 24*) where a low angle in-sequence formed thrust has been reactivated as a low angle normal fault. However, it is possible that in the case of this experiment, conditions were met just right in terms of the positioning of one of these thrusts over the velocity discontinuity in the setup.

Continuation of these type of setups in experiments D11 and D12 did in fact not yield similar results (*figs. 27 & 29*) and show that in the case where topography is removed and additional sand is added to simulate Paleozoic sedimentation, none of the thrusts created during compression are reactivated. This can either be attributed to the thrust sheets not being in the correct position over the velocity discontinuity or that the structural weaknesses formed by the thrust faults have been diminished by compaction due to the additional load of the sand before extension. It is however interesting to note that experiment D12 (*fig. 29*), where removal of topography was done continuously during the course of the experiment, a single thrust formed in a direction opposite to those of experiments D10 and D11 with a very strong listric nature, which might suggest that any major crustal compressional structures associated with the coalescing of Baltica and Avalonia may have been formed as curved planar features.

6.3 Crustal scale deformation

Assuming that the detachment between the Baltica Margin and the collapsed accretionary complex along which the Dutch Central Graben was created as a thrust at crustal scale in a ramp-flat-ramp geometry (Lyngsie and Thybo, 2007), reconstruction of this geometry should give an average slope of the ramp over which extension took place. As discussed in chapter 3 reconstruction of the interpreted MONA LISA-3 profile produced an average ramp of 12° (*fig. 32*), which is similar to the 14° found by (Williamson et al., 2002).
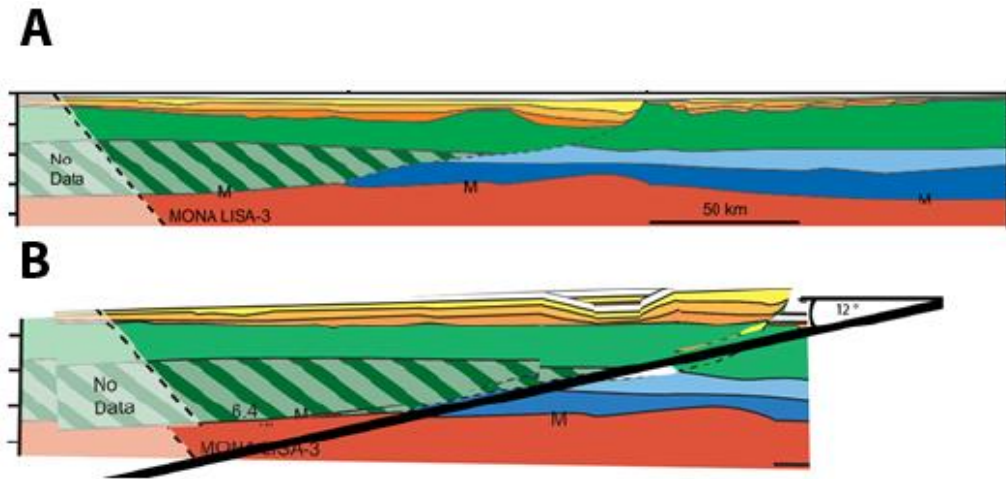
Figure 32 A) Interpreted MONA LISA-3 profile of present situation obtained from (Smit et al., 2016)**. B) Reconstructed MONA LISA-3 profile with 12° average detachment angle.**

Experiments D14 and D16 used this ramp in their setup and showed that when applying, deformation occurred as an overall graben geometry (*fig. 33*) at the junction between the brittle-ductile interface and the surface of the ramp, which suggests that the interplay between a preexisting ramp like structure and the interface between the brittle upper crust and ductile lower crust of Avalonia determined the placement of the Dutch Central Graben. The results of experiment D16 (*fig. 33*) show this very well. The plastic basal sheet that normally would be placed under the entirety of the putty, was removed in D16. During the experiment the graben would form at the same location as D14 with the plastic sheet, which further proves that the location of deformation taking place is solely influenced by the contact between the brittle-ductile interface and the surface of the ramp.
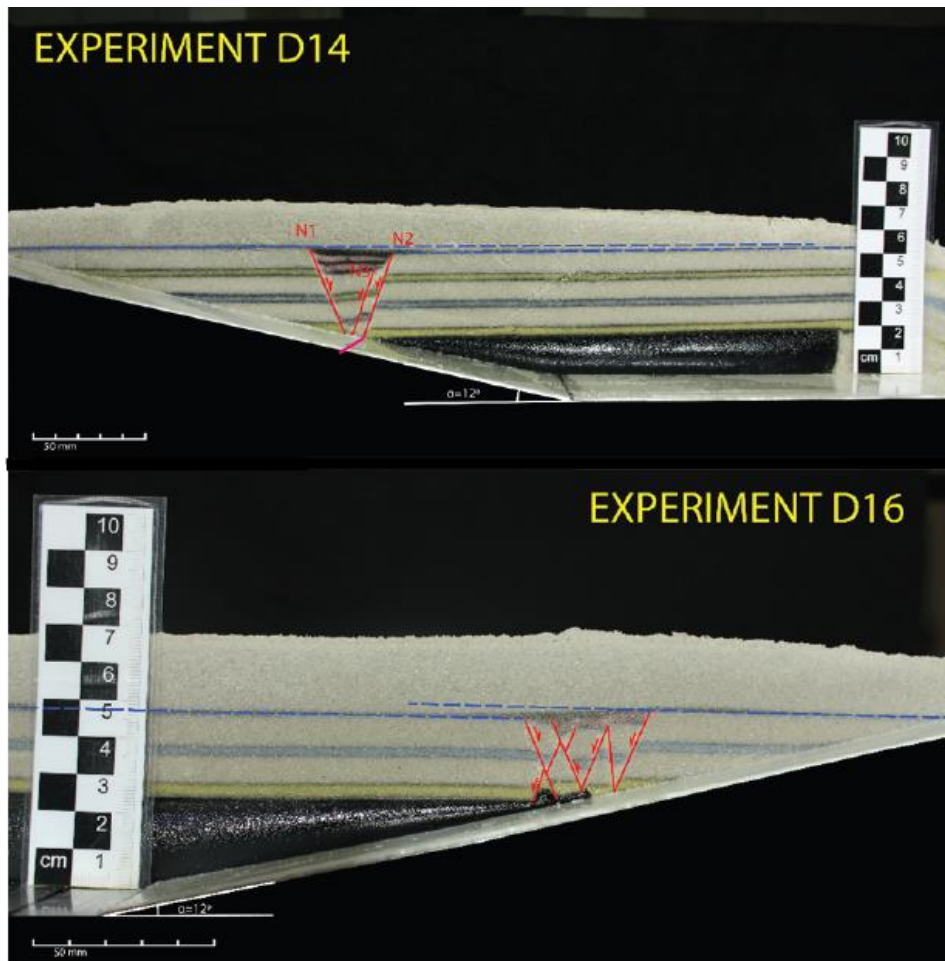
Figure 33 Cross-sections of experiments D14 and D16 showing that without a plastic basal sheet (purple line in D14) deformation is still concentrated at the junction between the ramp and the brittle-ductile interface

7. Main Conclusions

From the results obtained from analogue tectonic modelling and integrating these with work done by previous studies about the Dutch Central graben, the following conclusions can be made:

- Analogue tectonic modelling shows that when applying extension over a listric ramp, results show a striking similarity to nature in terms of the geometry and distribution of faulting and overall basin geometry. This suggests that the opening of the Dutch Central Graben during the Mezozoic was governed by a preexisting planar detachment surface of pre-Permian age. This structure that binds the DCG to the east is at present likely to be represented by the Coffee Soil Fault.
- This detachment formed through the reactivation of a thrust sheet, which is likely to be the remnant of a Caledonian orogenic complex that marks the suture between Avalonia and Baltica.
- While the reactivation of thrust sheets into low angle normal faults proved to be difficult to recreate using analogue modelling, natural examples of this are plentiful, which suggests that the methods used in this study to model negative inversion of thrust sheets are not suffice.
- Analogue modelling on a basin scale also shows that the location and opening of the Dutch Central Graben was determined by the junction between the Avalonia-Baltica suture and the brittle-ductile interface of the Avalonian crust.

8. Acknowledgements

References

Berthelsen, A., 1998, The tornquist zone northwest of the carpathians: An intraplate pseudosuture: Gff, v. 120, p. 223–230, doi:10.1080/11035899801202223.

Brun, J. –P., 1999, Narrow rifts versus wide rifts: inferences for the mechanics of rifting from laboratory experiments (R. S. White, R. F. P. Hardman, A. B. Watts, & R. B. Whitmarsh, Eds.): Philosophical Transactions of the Royal Society of London. Series A: Mathematical, Physical and Engineering Sciences, v. 357, p. 695–712, doi:10.1098/rsta.1999.0349.

Byerlee, J., 1978, Friction of rocks, *in* Pure and Applied Geophysics PAGEOPH, Basel, Birkhäuser Basel, v. 116, p. 615–626, doi:10.1007/BF00876528.

Cocks, L.R.M., and Torsvik, T.H., 2007, European geography in a global context from the Vendian to the end of the Palaeozoic: Geological Society, London, Memoirs, v. 32, p. 83–95, doi:10.1144/gsl.mem.2006.032.01.05.

Colletta, B., Letouzey, J., Pinedo, R., Ballard, J.F., and Bale, P., 1991, Computerized X-ray tomography analysis of sandbox models: examples of thin-skinned thrust systems: Geology, v. 19, p. 1063–1067, doi:10.1130/0091-7613(1991)019<1063:CXRTAO>2.3.CO;2.

Davy, P., and Cobbold, P.R., 1991, Experiments on shortening of a 4-layer model: Tectonophysics, v. 188, p. 1–25, https://www.sciencedirect.com/science/article/pii/004019519190311F (accessed February 2019).

Evans, B., and Goetze, C., 1979, The temperature variation of hardness of olivine and its implication for polycrystalline yield stress: Journal of Geophysical Research, v. 84, p. 5505, doi:10.1029/JB084iB10p05505.

Geluk, 2005, Stratigraphy and tectonics of Permo-Triassic basins in the Netherlands and surrounding areas: s.n.], https://dspace.library.uu.nl/handle/1874/1699 (accessed April 2019).

Gibbs, A.D., 1984, Structural evolution of extensional basin margins: Journal of the Geological Society, v. 141, p. 609–620, doi:10.1144/gsjgs.141.4.0609.

Graveleau, F., Malavieille, J., and Dominguez, S., 2012, Experimental modelling of orogenic wedges: A review: Tectonophysics, v. 538–540, p. 1–66, doi:10.1016/j.tecto.2012.01.027.

Lyngsie, S.B., and Thybo, H., 2007, A new tectonic model for the Laurentia-Avalonia-Baltica sutures in the North Sea: A case study along MONA LISA profile 3: Tectonophysics, v. 429, p. 201–227, doi:10.1016/j.tecto.2006.09.017.

Lyngsie, S.B., Thybo, H., and Rasmussen, T.M., 2006, Regional geological and tectonic structures of the North Sea area from potential field modelling: Tectonophysics, v. 413, p. 147–170, doi:10.1016/J.TECTO.2005.10.045.

Mona Lisa Working Group, 1997a, Closure of the Tornquist sea: Constraints from MONA LISA deep seismic reflection data: Geology, v. 25, p. 1071–1074, doi:10.1130/0091-7613(1997)025<1071:COTTSC>2.3.CO;2.

Mona Lisa Working Group, 1997b, MONA LISA—Deep seismic investigations of the lithosphere in the southeastern North Sea: Elsevier, https://www.sciencedirect.com/science/article/pii/S0040195196001114 (accessed December 2018).

Smit, J., 2005, Brittle-ductile coupling in thrust wedges and continental transforms:, https://www.narcis.nl/publication/RecordID/oai:research.vu.nl:publications%2F9df44171-0d55-48b2-988d-56bf6d826e98 (accessed February 2019).

Smit, J.H.W., Brun, J.P., and Sokoutis, D., 2003, Deformation of brittle-ductile thrust wedges in experiments and nature: Journal of Geophysical Research: Solid Earth, v. 108, doi:10.1029/2002JB002190.

Smit, J., van Wees, J.D., and Cloetingh, S., 2016, The Thor suture zone: From subduction to intraplate basin setting: Geology, v. 44, p. 707–710, doi:10.1130/G37958.1.

Torsvik, T.H., and Rehnström, E.F., 2003, The Tornquist Sea and Baltica–Avalonia docking: Tectonophysics, v. 362, p. 67–82, doi:10.1016/S0040-1951(02)00631-5.

Torsvik, T.H., Smethurst, M.A., Meert, J.G., Van der Voo, R., McKerrow, W.S., Brasier, M.D., Sturt, B.A., and Walderhaug, H.J., 1996, Continental break-up and collision in the Neoproterozoic and Palaeozoic — A tale of Baltica and Laurentia: Earth-Science Reviews, v. 40, p. 229–258, doi:10.1016/0012-8252(96)00008-6.

Van Wijhe, D.H., 1987, Structural evolution of inverted basins in the Dutch offshore: Tectonophysics, v. 137, p. 171–219, doi:10.1016/0040-1951(87)90320-9.

Williamson, J.P., Pharaoh, T.C., Banka, D., Thybo, H., Laigle, M., and Lee, M.K., 2002, Potential field modelling of the Baltica–Avalonia (Thor–Tornquist) suture beneath the southern North Sea: Tectonophysics, v. 360, p. 47–60, doi:10.1016/S0040-1951(02)00346-3.

van Winden, M., de Jager, J., Jaarsma, B., and Bouroullec, R., 2018, New insights into salt tectonics in the northern Dutch offshore: a framework for hydrocarbon exploration: Geological Society, London, Special Publications, v. 469, p. 99–117, doi:10.1144/SP469.9.

Wong, T.E., Batjes, D.A.J., and Jager, J., 2007, Geological development, *in* Amsterdam, Royal Netherlands Academy of Arts and Sciences.

Ziegler, P., 1990a, Geological Atlas of Western and Central Europe, Shell Internationale Petroleum Maatschappij BV/Geological Society of London:

Ziegler, P.A., 1992, North Sea rift system: Tectonophysics, v. 208, p. 55–75, doi:10.1016/0040-1951(92)90336-5.

Ziegler, P.A., 1990b, Tectonic and palaeogeographic development of the North Sea rift system. In: Blundell, D.J. & Gibbs, A.D. (eds) Tectonic evolution of the North Sea rifts: Oxford University Press, p. 1–36, https://scholar.google.nl/scholar?hl=nl&as_sdt=0%2C5&q=Tectonic+and+palaeogeogr ahic+development+of+the+North+Sea+rift+system.&btnG= (accessed December 2018).

Ziegler, P.A., and Kent, P., 1982, Faulting and Graben Formation in Western and Central Europe [and Discussion]: Philosophical Transactions of the Royal Society A: Mathematical, Physical and Engineering Sciences, v. 305, p. 113–143, doi:10.1098/rsta.1982.0029.